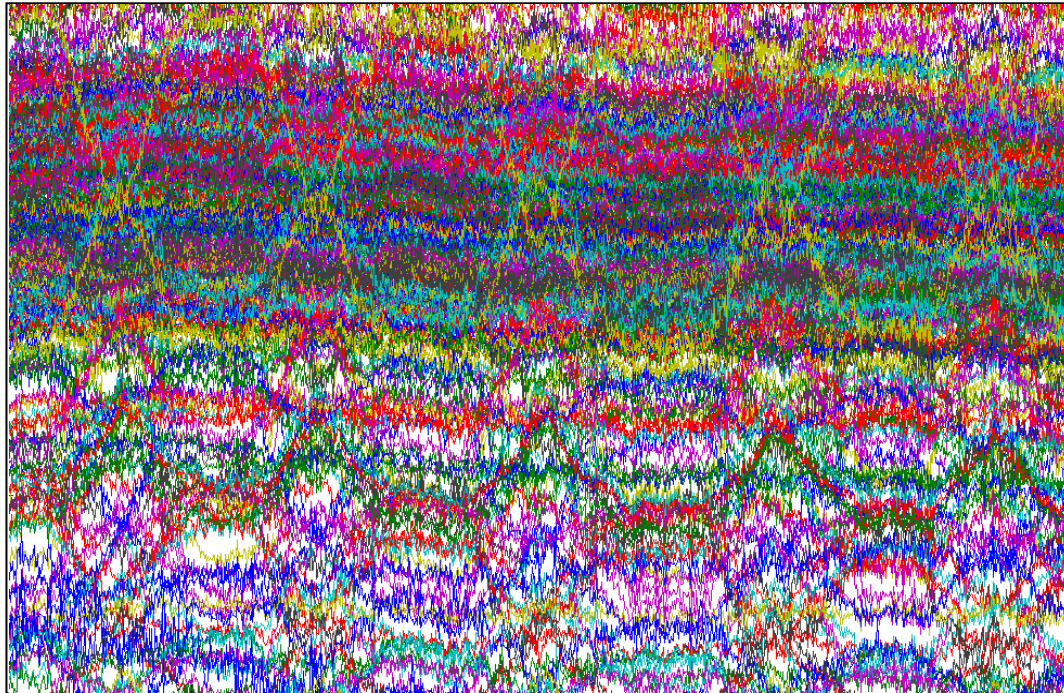


CHALMERS



Application Development on Compact UWB Radar Systems

*Master of Science Thesis [in the Master Degree Programme, Biomedical
Engineering]*

QIUCHI JIAN

Department of Signal and Systems
CHALMERS UNIVERSITY OF TECHNOLOGY
Gothenburg, Sweden, 2014
Report No. EX021/2014

Application Development on Compact UWB Radar Systems

QIUCHI JIAN

Department of Signal and Systems

CHALMERS UNIVERSITY OF TECHNOLOGY

Göteborg, Sweden, 2014

Ultra-wide band radar signal processing

© QIUCHI JIAN, 2013

Master's Thesis EX021/2014

Department of Signal and Systems
Chalmers University of Technology
SE-41296 Göteborg
Sweden

Ultra-wide band radar signal processing
Master's Thesis in the Master's programme in Biomedical Engineering
QIUCHI JIAN
Department of Signal and Systems
Chalmers University of Technology

Abstract

Ultra-wideband (UWB) radar technique is widely used in various applications from different domains. The UWB radar system in this work consists of two (Tx and Rx) antennas and one compact CMOS UWB transceiver. For civilian applications by near field measurements, such as medical monitoring instruments, parking radars, or ranging and tracking systems, some desirable properties, including i) compact in size, ii) low cost, iii) fast processing speed, iv) high spatial resolution and v) high penetration abilities, have been achieved to a large extent by the system presented in this thesis. This Master project emphasizes two aspects: i) further investigation on the self-grounded bowtie antenna by using numerical simulations; and ii) development of signal processing techniques for applications such as breathing and heartbeat monitoring for medical purposes and sand flow detection for road sanding.

Index Terms: self-grounded bow-tie antennas; UWB radar application; wavelet; Empirical Mode Decomposition, breathing monitoring; heartbeat detection; sand flow detection

Acknowledgments

I would like to thank everyone involved in this thesis work from both Chalmers University of Technology and Imego Institute.

To my thesis examiners: Associated Professor Jian Yang, Professor Tomas McKelvey from Chalmers University of Technology, and Dr. Peter Björkholm from Imego Institute, for their patience in supervisions and the guidance not only about the thesis work, but also in the philosophy of scientific research;

To PhD student Yinan Yu from Chalmers University of Technology, for her tremendous help and continuous encouragement during the work. All this work would not have been possible without her support;

To Dr. Borys Stoew from Imego Institute, for his kind support. His wide knowledge in many aspects inspired me deeply. It is a great honor to be instructed by him.

To my colleges in Imego Institute, for the help for daily work. I really appreciate the memorable time we spent together.

Finally, I would like to thank my parents, without their endless love and selfless support, I would never be able to come so far in my education. I am forever grateful for what you have done for me.

List of Abbreviations

API	Application Programming Interfaces
CST MWS	Computer Simulation Technology Microwave Studio
CR	Corner Reflector
EMD	Empirical Mode Decomposition
FCC	Communications Commission
IMF	Instantaneous Mode Functions
MS	Magnetic Shielded
Rx	Receiving Antenna
SVD	Singular Value Decomposition
Tx	Transmission Antenna
UWB	Ultra-wideband

Table of Contents

1	Introduction	1
1.1	Ultra-wideband Radar	1
1.2	Goal and Tasks	1
2	Self-grounded Bow-tie Antenna Simulation	3
2.1	Simulation Environment and Models	3
2.2	Results and Analysis	4
3	System Calibration	7
3.1	System Structure and Parameters	7
3.1.1	Antennas	7
3.1.2	Radar Module	8
3.1.3	Parameters in the Measurement	8
3.2	Raw Signal	10
3.3	Temperature Effect	11
3.4	Jamming	12
4	Breath Detection	15
4.1	System Setup and Measurement Methodology	15
4.2	Signal Processing	16
4.2.1	Signal Pre-processing	16
4.2.2	Motion Detection	17
4.2.3	Signal Extraction	19
4.2.4	Breath Signal Retrieval	20
4.3	Result and Discussion	21
5	Heart Rate Detection	23
5.1	Computer Simulation	23
5.1.1	System Modeling	23
5.1.2	Methodology	24
5.2	Experiment with Corner Reflector	32
5.2.1	Measurement Setup	32
5.2.2	Signal Processing	33
5.2.3	Result and Discussion	34
5.3	Measurement with Real Human	36
5.3.1	Motion Detection	36
5.3.2	EMD	37
5.3.3	Wavelet Packets	38

5.3.4	Result and Discussion.....	39
6	Sand Flow Detection	42
6.1	Experiment with Funnel	42
6.1.1	System Setup and Measurement Methodology	42
6.1.2	Results and Discussion	43
6.2	Measurement with Sand Box.....	45
6.2.1	System Setup and Measurement Methodology	45
6.2.2	Result and Discussion.....	45
7	Summary and Future Work.....	48
8	References.....	50
9	Appendix A: Demo system.....	52
9.1	Raw Data	52
9.2	Clutter Removal	53
9.3	One Dimension Tracking	54
9.4	Breath Detection.....	55
9.5	Heart Rate Detection	57
10	Appendix B: Paper Published in EuCAP 2014	59

1 Introduction

Ultra-wideband (UWB) radar technique has been widely used in various applications from different domains. This thesis work emphasizes the following two aspects:

- Further investigation of the self-grounded bowtie antenna by using a commercial EM (electromagnetic) solver – CST Microwave Studio;
- Development of Signal processing techniques for the applications such as breathing and heartbeat monitoring for medical purposes and sand flow detection for road sanding.

1.1 Ultra-wideband Radar

UWB technology has dramatically improved in the past years. In 2002, the Federal Communications Commission (FCC) formally defined the frequency, bandwidth among other respects with UWB. Besides that, FCC also classified the possible applications into different categories with constrains, such as data transmission and radar. [1][2]

Several distinct advantages make UWB radar systems attractive for many civilian applications by near field measurements, such as medical monitoring instruments, parking radars, or ranging and tracking systems [3]. Those advantages include [2][4]:

- Good time domain resolution that enables the UWB systems to have accurate tracking and positioning;
- Strengthened target recognition;
- Robust to passive jamming;
- Relatively low cost.

1.2 Goal and Tasks

The goal of this project is to develop different prove concept applications with UWB radar systems based on its advantages. Through this thesis project, the working principle of UWB radar system has been studied and the possibilities of different UWB radar applications have been developed. Following tasks have been done:

- Computer Simulation Technology Microwave Studio (CST MWS) is used for simulation for self-grounded Bow-tie antenna with different target surfaces;
- Breath detection;
- Simulations, experiments and real heart rate detection;
- Experiments and real sand flow detection;
- A demo system for possible applications with UWB radar system.

2 Self-grounded Bow-tie Antenna Simulation

In order to understand the behaviour of the self-grounded bow-tie antenna which is a compact UWB antenna with many applications [5]-[10], a set of models for different scenarios of a self-grounded bow-tie antenna are simulated and analysed using CST MWS.

2.1 Simulation Environment and Models

Six models, referred to as models 1 to 6, with different setups have been run successfully with 10ns steady time. A self-grounded bow-tie antenna is used in all models, and, as shown in Table 1, each model has its own environment setup in order to simulate different measurements: model 1 has only the antenna; models 2 and 3 have an iron surface placed toward the antenna with different distances; models 4 to 6 have different surface conditions: surface covered by water layer, water drops and ice layer. Figure 2-1 is the screen shot of one of those simulation models.

Table 1 Setup of simulation models

Model #	1	2	3	4	5	6
Antenna Size						
Face to an Iron Surface	No	Yes				
Surface Size	N/A	x:-500~500; y: -500~500; z: -10~0.				
Surface Property	N/A	Electric Conductivity: 1.04e+007; Mue: 1.				
Dis. from Antenna(mm)	N/A	300	600	300		
Covered by	N/A			Water	Water Drops	Ice

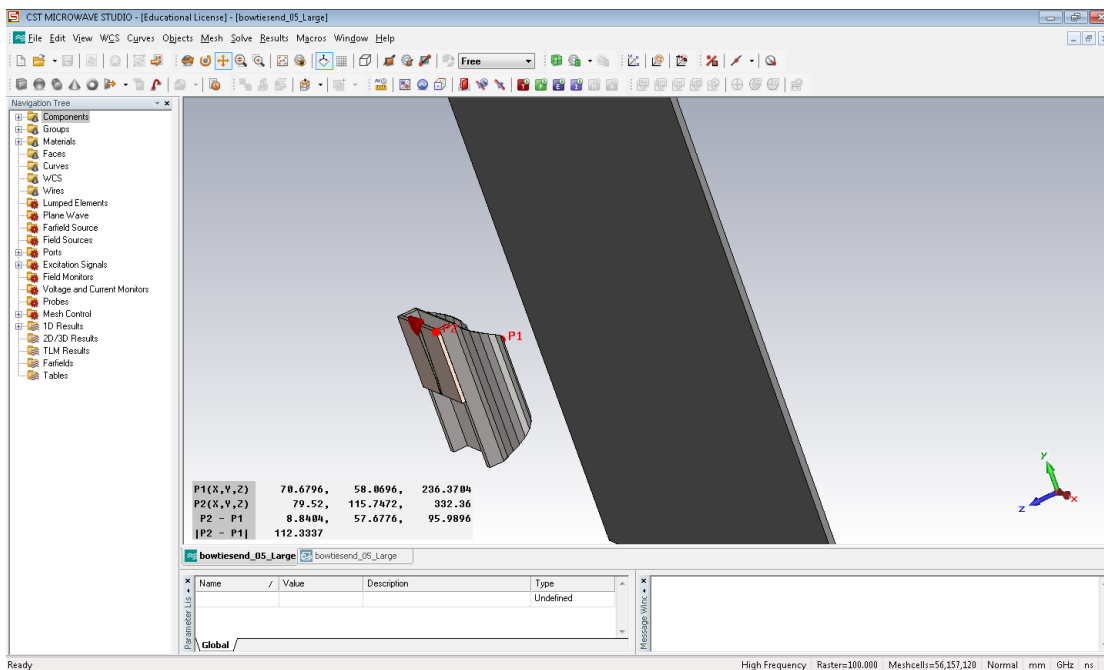


Figure 2-1 Screen shot of a simulation model

2.2 Results and Analysis

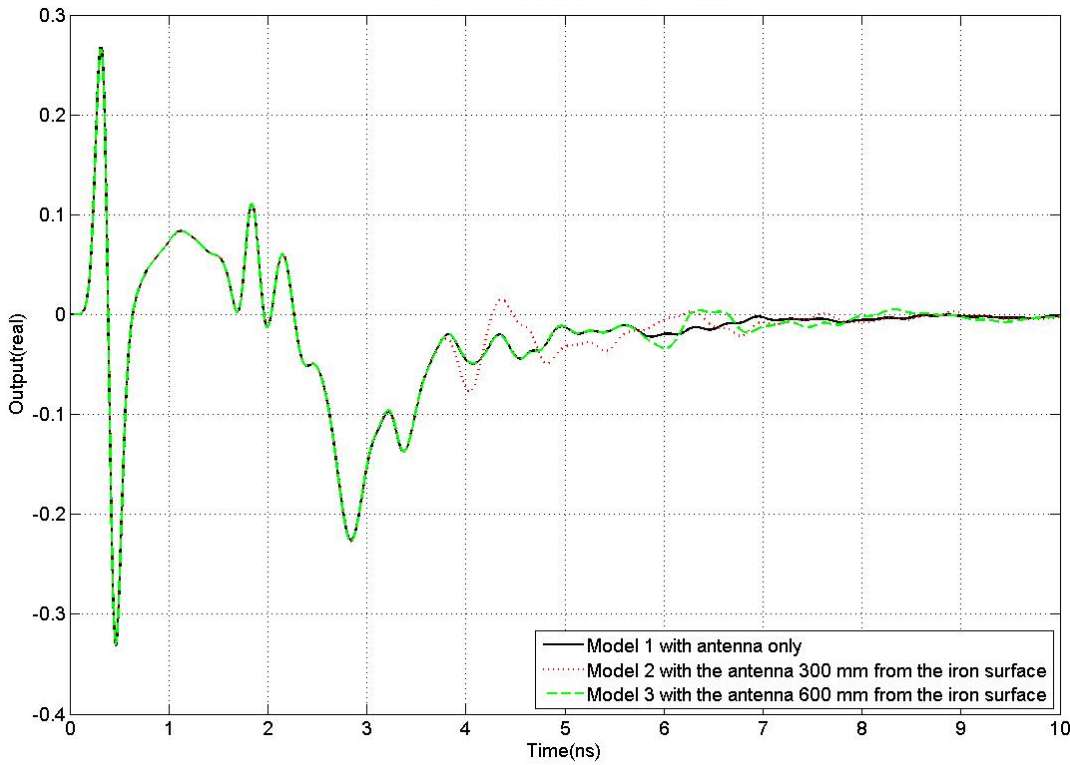


Figure 2-2 Results from model 1, 2 and 3 in time domain

Figure 2-2 contains the results from the first 3 models. The curve in black is from the model with a self-grounded bow-tie antenna only. The dotted lines in red and green are from models with the distance 300mm and 600mm between the antenna and the iron surface, respectively. It can be seen from the graph that all 3 curves coincide from the start to about 3.5 ns. After that, the red and the green dotted lines deviate from the black curve at around 3.8 and 5.8 ns, respectively.

In order to remove the interference from the antenna itself, the signal from model 1 is used as a clutter map. In Figure 2-3, the red curve and the blue dotted curve are made by subtracting the clutter map from the signal from model 2 and model 3, respectively. By the setup of these simulation models, it is clear that the reflection should be received after time t_r , which could be calculated by

$$t_r = t_a + t_{incident} + t_{reflection} \quad (2.1)$$

where t_a is the time the signal traveling inside the antenna (cable is included), $t_{incident}$ and $t_{reflection}$ are the time that the signal travels to and from the iron surface. Considering there is only one antenna in our setup and all objects remain still, the $t_{incident}$ and $t_{reflection}$ should always be the same, and the traveling time in the air could be calculated by traveling distance over $3 * 10^{11}$ mm/s, the equation could reduce to

$$t_r = t_a + 2 * \frac{d_{target}}{3 * 10^{11} \text{ mm/s}} \quad (2.2)$$

Therefore, the t_r of the red curve is

$$t_{r_{red}} = t_a + 2 * \frac{300 \text{ mm}}{3 * 10^{11} \text{ mm/s}} = t_a + 2 \text{ ns} \quad (2.3)$$

And the t_r of the green curve is

$$t_{r_{blue}} = t_a + 2 * \frac{600 \text{ mm}}{3 * 10^{11} \text{ mm/s}} = t_a + 4 \text{ ns} \quad (2.4)$$

Thus, the difference of the reflection time between the blue and the red curve should be 2ns. As we can see from Figure 2-3, the distance between the main peak of the red curve and the blue one is around 2 ns, which concurs our theoretical calculation. Besides that, a significant attenuation of signal strength with the increasing distance between the antenna and the target can also be observed from the figure.

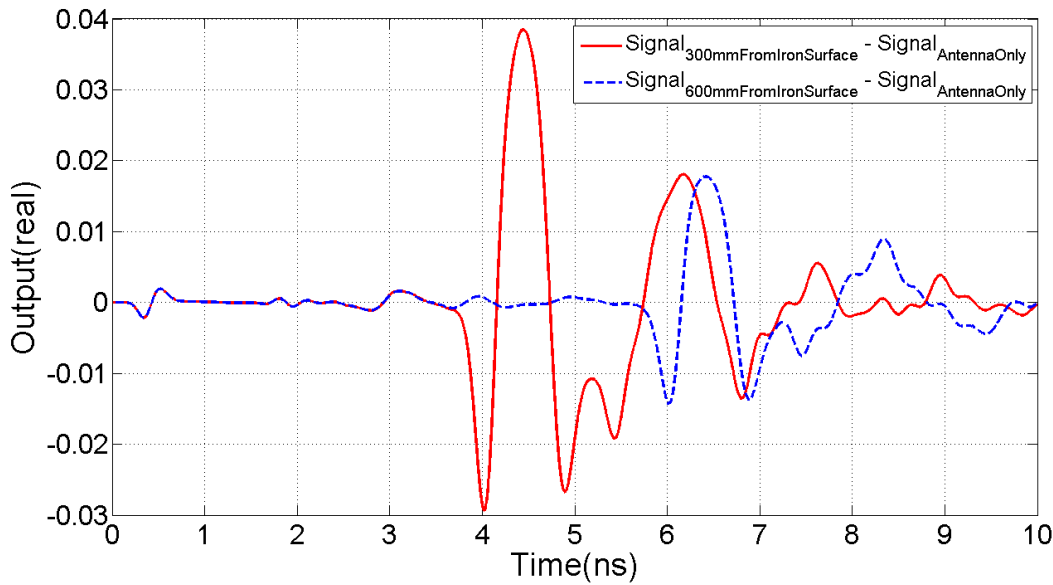


Figure 2-3 Clutter removed results from model 2 and 3 in time domain

Figure 2-4 contains the results in frequency domain from all models but model 2. The reference curve here is the black curve from model 1, which contains only the antenna. The rest models have both the antenna and a surface placed 300mm from the antenna with different conditions, such as iron surface, water layer covered iron surface and so on. Based on the shape of these curves, we could divide them into two groups, where group A contains model 3 and 4, and group B contains model 5 and 6.

The two curves in group A share some features with the black curve on the shape, but with significant magnitude differences especially in the range of 0.5 to 1.8 GHz. These differences could be useful for distinguishing surface conditions. On the other hand, the curves from group B are quite different from the reference curve. Therefore, it should be possible to make a distinction between these two conditions and the model 1. Considering the temperature could be good reference information, although these two curves share high similarity with each other, it is possible to determine the surface conditions.

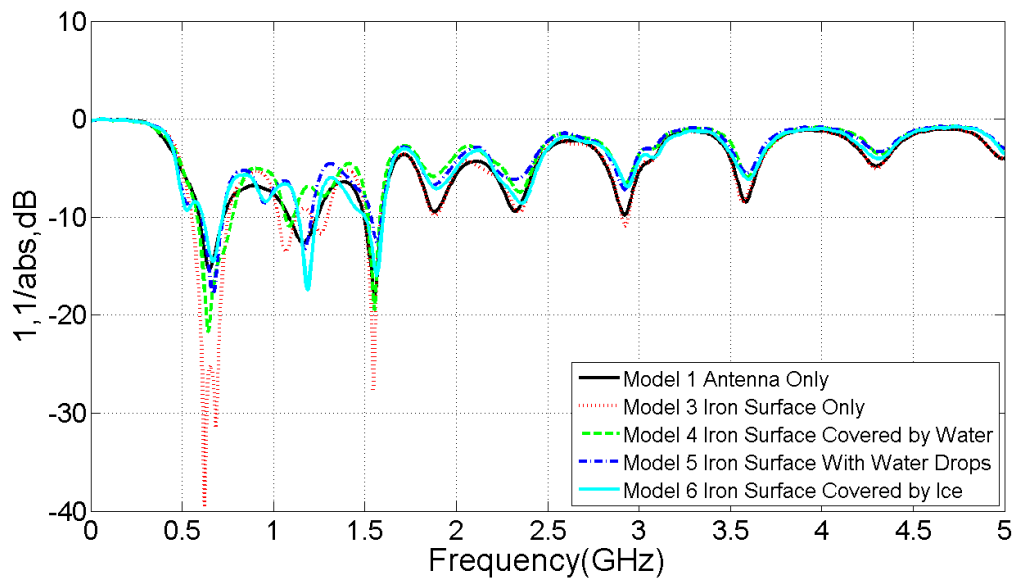


Figure 2-4 Results of all models except model 2 in frequency domain

3 System Calibration

System calibration is applied to clarify the system property and identify potential interferences that could compromise the measurements, such as temperature effect and jamming. Adjustments corresponding to what have been done on the further experiment environment setups.

3.1 System Structure and Parameters

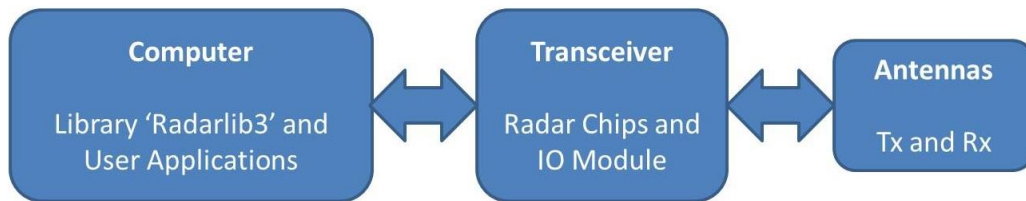


Figure 3-1 Structure diagram of the radar system

Figure 3-1 shows the structure of the radar system that is used in this work. The system is mainly composed of a computer, a Novelda transceiver, a transmission antenna (Tx) and a receiving antenna (Rx). The antennas are connected to the transceiver through SMA (subMiniature version A) connectors and the transceiver is connected to the computer via a USB cable. Signal and transceiver parameter acquisition and update is done through Application Programming Interfaces (APIs) that are provided by Novelda’s library Radarlib3. [RadarUserGuide]

3.1.1 Antennas

Antennas used in this project are mainly Vivaldi 004 and Vivaldi 006, as shown in Figure 3-2. Table 2 contains some properties of these antennas:

Table 2 Main parameters of antennas [11][12]

	Dimensions	Frequency band
Vivaldi 004	150mmx133mmx1.6 mm	900 MHz – 5 GHz
Vivaldi 006	52mmx52mmx1.52 mm	3 – 20 GHz



Figure 3-2 Photos of antennas. From left to right: the front side of the Vivaldi 004 antenna; the back side of the Vivaldi 004 antenna; the front side of the Vivaldi 006 antenna; and the back side of the Vivaldi 006 antenna.[11][12]

3.1.2 Radar Module

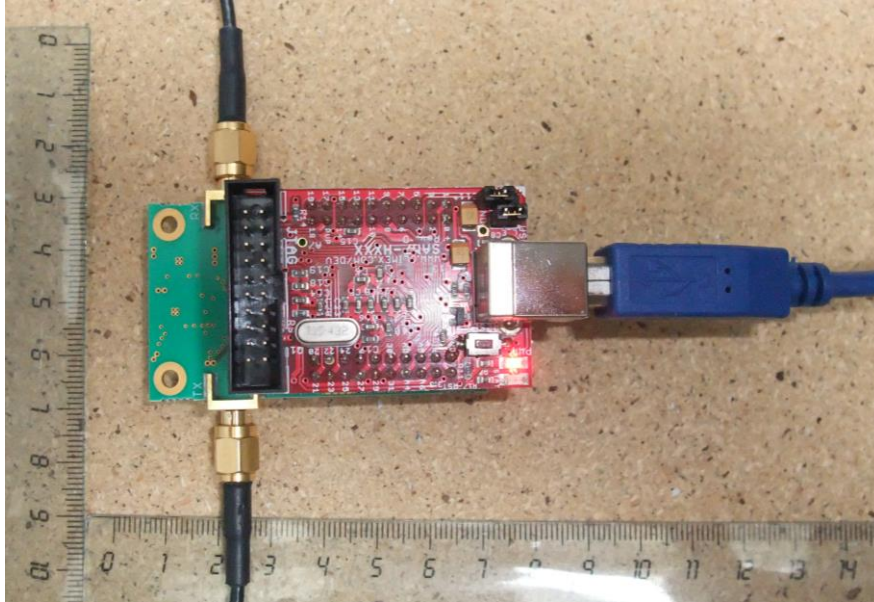


Figure 3-3 Photo of the Novelda radar module

Novelda radar module contains a NBA6100 chip with transmit bandwidth from 450MHz to 3.55GHz, a flash for storing data, a USB2.0 IO module as power supplier as well as data communicator to computer with a data rate of 480Mb/s speed [15].

3.1.3 Parameters in the Measurement

Table 3 contains some parameters that are used in the measurements in this work.

Table 3 Novelda radar system parameters [15]

Parameter Name	Description	Value
Averaging Factor (AF)	The number of internal samples is taken before output, which affects the processing speed and the noise level.	100
Gain	The gain of the transmitted signal.	5
Frame Offset (FO)	Internal time delay (including both antennas and cables): decides the range of the view for the radar.	290(Vivaldi004) 278(Vivaldi006)

Pulse Repetition Frequency (PRF)	The frequency the pulses are sent.	48 MHz
DAC	Digital to analog Converter. Convert the signal to 13 bits.	8192
Distance resolution (DS)	Distance between each sampler.	3.7137 mm (in air)
Samplers Per Frame (SPF)	The number of samplers in each frame.	512
Range	The maximum distance the radar could detect, with the FO setting, the range could be calculated by $\text{Range} = \text{DS} * \text{SPF}$.	From the outer edge of the antenna extends to about 1.9 m (in air)
Frame Rate (FR)	The number of frames that could be obtained per second, could be calculated by $\text{FR} = \text{PRF} * \frac{1}{\text{DAC} * \text{AF}}$.	≈ 59 frames/s theoretically, the real frame rate depends on the condition of the computer.

3.2 Raw Signal

The NVA6100 radar module supports sampling window with 512 parallel samplers [15]. Therefore, data from each sampling window is a 512 elements vector, which is called as a frame of signal. As shown in Figure 3-4, a frame of signal collected at time t is represented by a vector r , and each element in the vector, which is represented by $r(i)$, is the data from sampler i at time t . The frame's view can describe the environment regarding the distance from the antenna at certain time t .

	Sampler 1	Sampler 2	Sampler 3	...	Samper 511	Samper 512
t	$r(1)$	$r(2)$	$r(3)$...	$r(511)$	$r(512)$

Figure 3-4 An example of a frame of data that is collected at time t

By collecting signals over time, a signal matrix X , as shown in Figure 3-5, can be constructed. In the figure, the sampling time is represented by from t_1 to t_n . The data $X(t, s)$ represents the data collected by sampler s at time t . Besides the frame's view, with a data matrix, it is also possible to observe the changes on a specific sampling point among time, which is called sampler's view. Different from the frame's view, which can reflect the changes in certain range, the sampler's view focus more on the changes at a fixed position. Based on the different properties of these two views, a more comprehensive observation can be obtained.

	Sampler 1	Sampler 2	Sampler 3	...	Samper 511	Samper 512
t_1	$X(1,1)$	$X(1,2)$	$X(1,3)$...	$X(1,511)$	$X(1,512)$
t_2	$X(2,1)$	$X(2,2)$	$X(2,3)$...	$X(2,511)$	$X(2,512)$
t_3	$X(3,1)$	$X(3,2)$	$X(3,3)$...	$X(3,511)$	$X(3,512)$
...
t_n	$X(n,1)$	$X(n,2)$	$X(n,3)$...	$X(n,511)$	$X(n,512)$

Figure 3-5 An example of a data matrix that is collected from time t_1 to t_n

3.3 Temperature Effect

During the system calibration, by looking into the sampler's view of raw signal, it is observed that there is a heating effect in the system. This could be due to the temperature of the chip raises rapidly in the first period of the measurement. In order to determine the time it takes to reach a stable level, several measurements are done.

All measurements are done in a still environment with heating time from 0s to 900s. The results from three measurements with start-up time 0, 90 and 180 seconds are shown in Figure 3-6. It can be seen from the figure that in the first 60 seconds, the signals from each sampler are affected by the temperature effect significantly. However, after around 90 seconds, the signal could get over the temperature effect.

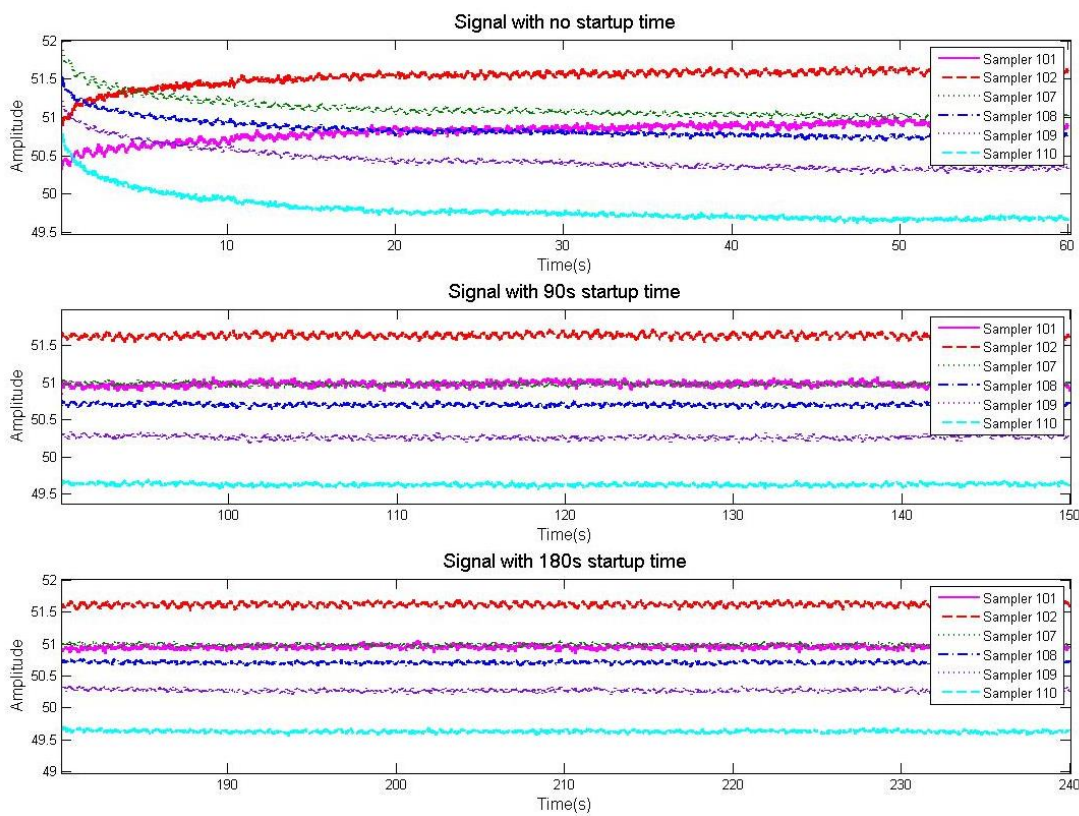


Figure 3-6 The raw signal from several samplers with different start-up times in the sampler's view.

3.4 Jamming

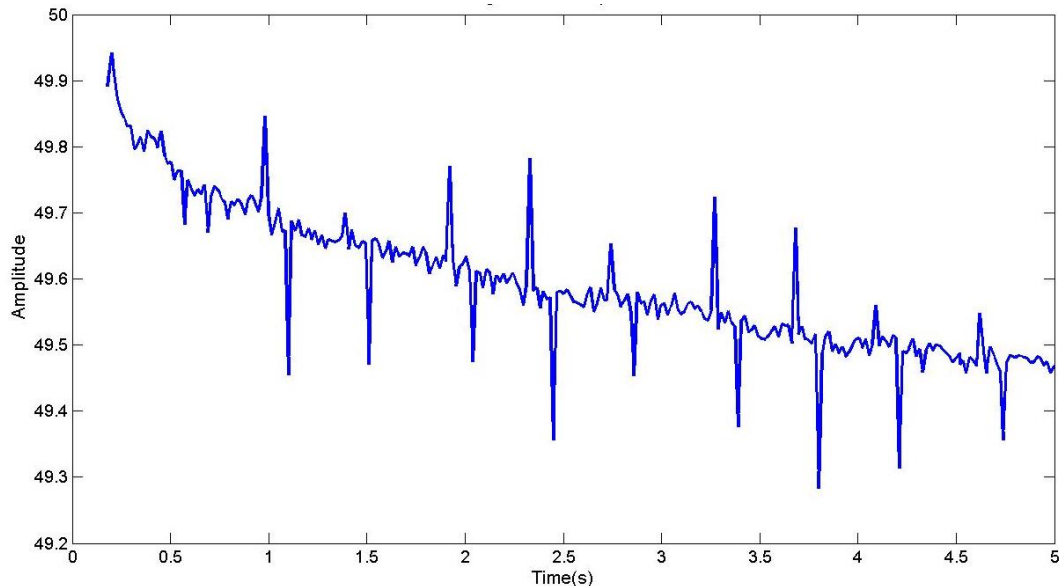


Figure 3-7 The raw signal from the 20th sampler during 5 seconds period.

From the analysis of measurements, it is clear that there is some unknown interference with certain pattern in the signal. Some more data were collected in the same place with no moving object.

The Figure 3-7 above shows the signal from the twentieth sampler in the frame for five seconds. As we can see, there are some pluses with frequency around 2 Hz. Considering in this study, the signals with lower frequencies are the main interest, such interference might significantly affect our observation. Therefore, it is important to find out the possible interference source.

Above all, the power frequency could be ruled out. This is because not only that the plot shows much lower frequency, but also because the sampling rate is around 60 Hz, which is far below the minimum sampling frequency that defined by Nyquist–Shannon sampling theorem.

The noise is highly possible emitted from some device around, considering it has a very strong pattern. Thus, several measurements were done for verification with the setup in Table 4.

First of all, in order to exclude electromagnetic interference from the cables connecting the antennas, transceiver and computer, a shielding ring was used in different places for several measurements. The signal is affected very little by using a shielding ring on single wire between the transceiver and the antenna, or using it on both wires at the same time. Thus, the cables are not the major source.

Beside cables, the transceiver itself could be a source. By changing the sampling rate and PRF, the transceiver did sampling and generated pulses in different frequencies. However, the interference remained the same. Therefore, the transceiver should not be the source.

Table 4 Experiment setup for determining jamming source

Possible Source	Control Group Setup	Experiment Setup	Comparison result
SMA cables connecting to antennas	No shielding ring at all	Shielding ring on Tx cable	Have slightly difference
	No shielding ring at all	Shielding ring on Rx cable	Have slightly difference
	No shielding ring at all	Shielding ring on both cables at the same time	Hardly see any differences.
USB cables connecting to computer	No shielding ring at all	Shielding ring on the cable	Hardly see any differences.
Radar Module	Sampling rate set to 0	Sampling rate set to 1	Jamming is still there
	Sampling rate set to 0	Sampling rate set to 2	Jamming is still there
	PRF set to 48 MHz	PRF set to 6 MHz	Jamming is still there
	PRF set to 48 MHz	PRF set to 12 MHz	Jamming is still there
	PRF set to 48 MHz	PRF set to 24 MHz	Jamming is still there
Desktop Computer	System connected to a desktop computer	System connect to a laptop with plugin power source	Jamming is still there
	System connect to a laptop	System connect to a laptop with battery as power source	Jamming is still there

The next possible interference source device was the desktop computer. In order to eliminate the effect from it, a laptop computer with battery as power source was used for replacement. However, the interference still remained.

Considering all electronic devices in the room are excluded, the only possibility left is that the interference is from electromagnetic field generated somewhere else. Therefore, the radar system was moved to a magnetic shielded room and connected to a computer outside the room with the cable through a small hole on the wall. Following is the comparison of the result and it confirmed that the interference source is not from the system itself.

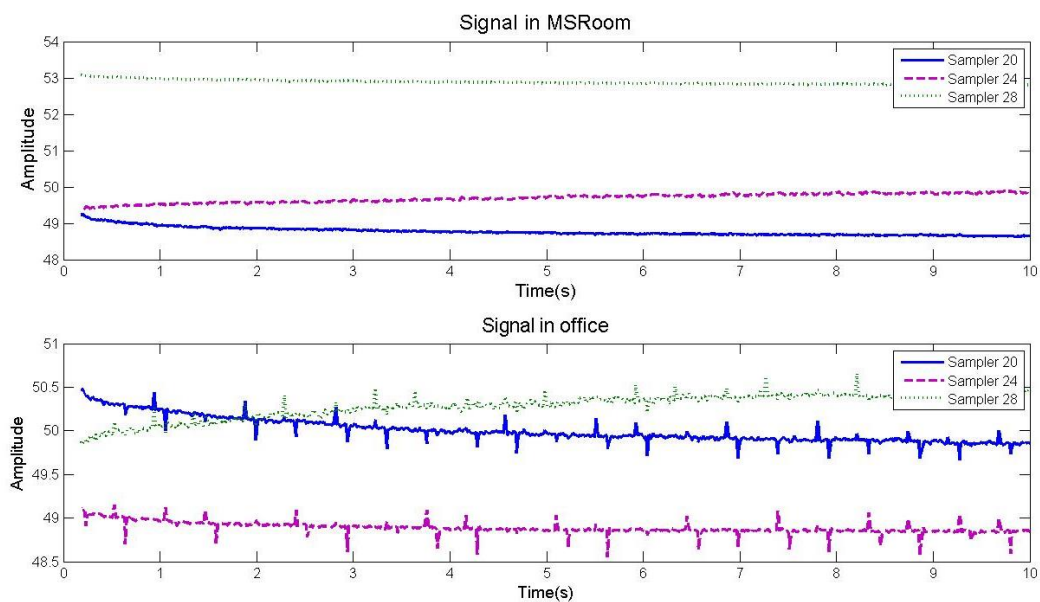


Figure 3-8 Raw signals from 3 samplers (20th, 24th, 28th) in a still environment in a magnetic shielded room and a normal office.

4 Breath Detection

4.1 System Setup and Measurement Methodology

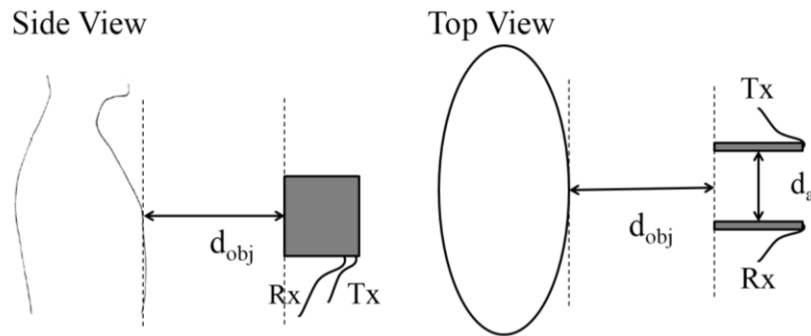


Figure 4-1 Diagram of the experimental setup of the breath detection using the present UWB radar system. The graph on the left hand side shows the setup from the side view and the right hand side one shows from the top view.

Figure 4-1 is the setup diagram for breathing detection: two Vivaldi 004 antennas Tx and Rx are placed in parallel with 12cm distance between each other, which is represented by d_a in the figure. One person is sitting still in a chair with a distance 24 cm, which is represented by d_{obj} in the figure, between the chest and the outer edge of the antennas. In the experiment phase, measurements have been done for 60 seconds continuously. From previous test, the frame offset should be 290 in order to set the detection range from the outer edge of the antennas.

4.2 Signal Processing

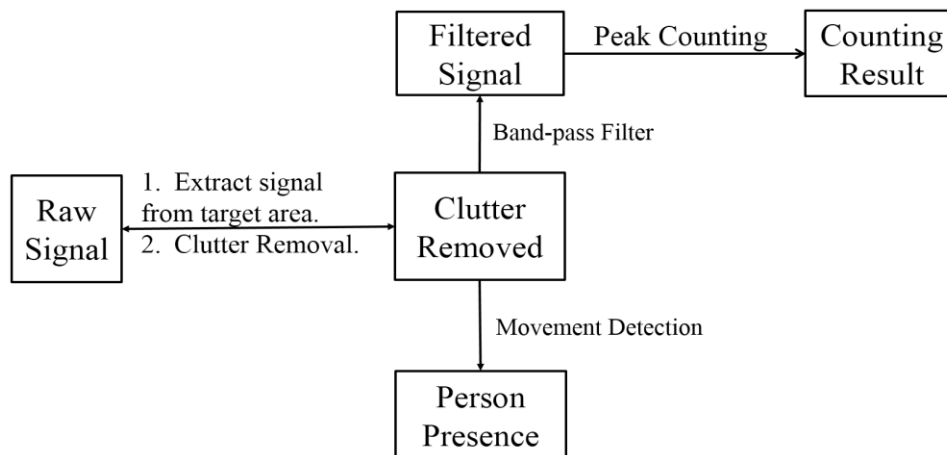


Figure 4-2 Signal processing procedure diagram for breath detection.

The Figure 4-2 is the flow chart of the signal processing procedures. The collected raw signal first passes the pre-processing procedure to extract signal from the target area, where contains the most interesting signal, and remove the clutter. After that, the signal is used for two purposes, one is to verify the target's presence, and the other is for retrieving the breath signal.

4.2.1 Signal Pre-processing

Considering the radar has a relatively wide range compared to the size of human's chest, only partial signal from the target area is taken for further process, which based on the distance between human and the antennas, for time gating the signal.

For example, the Figure 4-3 shows a frame of signal. During the measurement, the person was sitting about 240mm from the outer edge of the antennas. By the radar's distance resolution, which is 3.7137 mm, we deduce that the person should be in the area after sampler 65. Considering the human in the measurements has about 180 mm thick chest and taking possible measurement errors into account, target area was set to between sampler 55 and sampler 104 as showed in the figure in red.

After obtaining the data of interest, the clutter removal is followed. The previous developed singular value decomposition (SVD) method for clutter mapping [4] was used here. The outcome data was used for further processing.

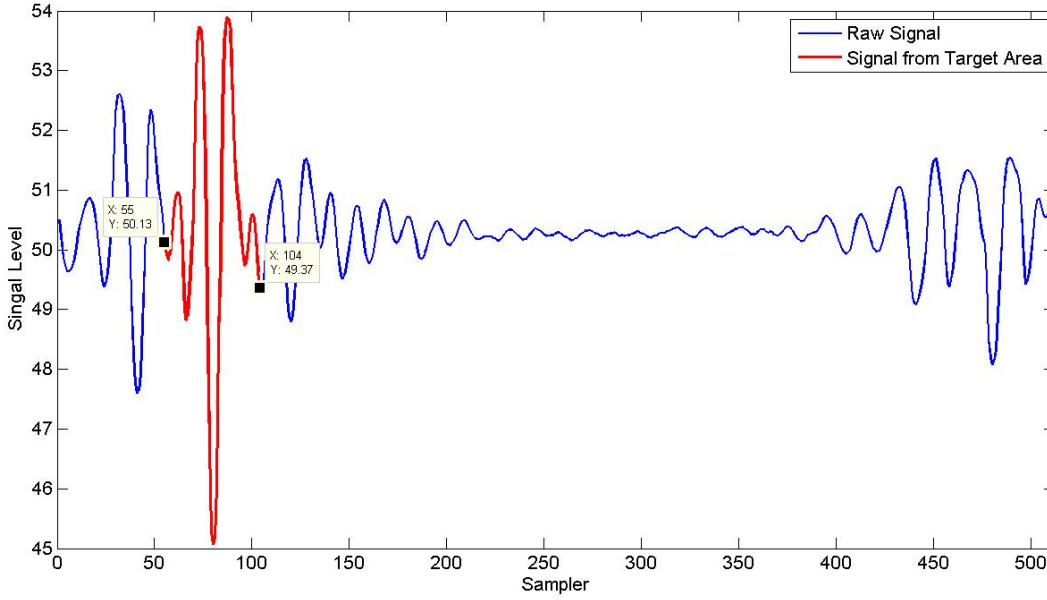


Figure 4-3 A frame of signal collected when there is a person in its detection range.

4.2.2 Motion Detection

In order to confirm the received signal contains information about any moving object, a differential phase method is applied here for motion detection. For two identical signals with a time delay, the time delay could be obtained by Fourier Transform. [4]

Suppose s_1 and s_2 are identical signals with a phase shift:

$$s_2(t) = s_1(t - \tau) \quad (4.1)$$

By applying Fourier Transform we have:

$$S_{1(\omega)} = S_{2(\omega)} e^{-j\omega\tau} \quad (4.2)$$

Therefore:

$$\frac{S_{1(\omega)}}{S_{2(\omega)}} = e^{-j\omega\tau} \quad (4.3)$$

Thus, the angle difference could be obtained by:

$$\angle \frac{S_{1(\omega)}}{S_{2(\omega)}} = -\omega\tau \quad (4.4)$$

Considering human breath is a slow periodic movement and the radar has a high sampling rate, in most of the samples, the target has either small movement or remain still comparing with the previous sample. Therefore, the distribution of the phase shift should have a very high peak around 0 and then drop dramatically on both sides. On the other hand,

in an environment with random noise, if there is nothing moving periodically in the detection range, the curve calculated with the measurement data would show a Gaussian distribution. Therefore, this could help us to detect the presence of target.

Figure 4-4 shows an example of motion detection. Two measurements were done with almost the same environment setup. The only difference is in the second measurement, there was a person sitting in the target area breath normally. The blue curve is calculated from the measurement data with no person presence and the red one is from the measurement data that one person was sitting in the range. As we can see from the figure, these two curves can be easily distinguished by both the peak value and the shape.

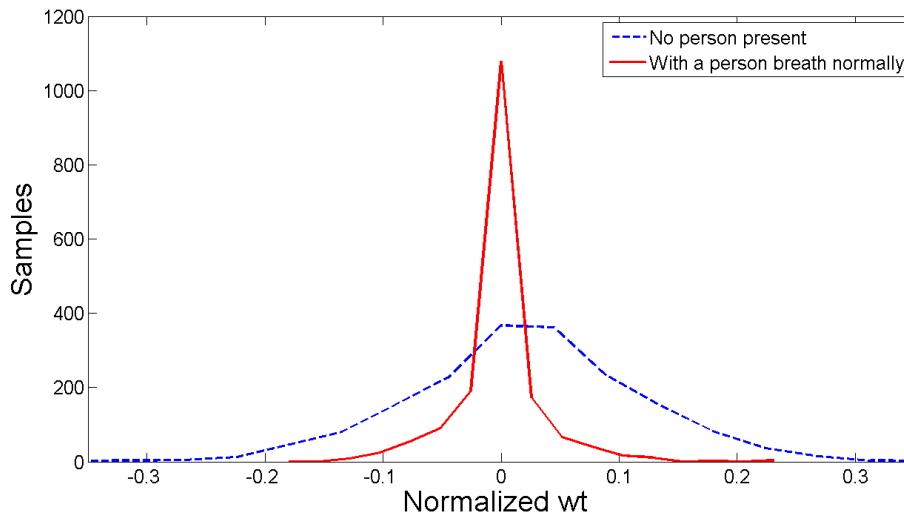


Figure 4-4 Calculation results based on the data collected with and without a person present in the radar's detection range.

4.2.3 Signal Extraction

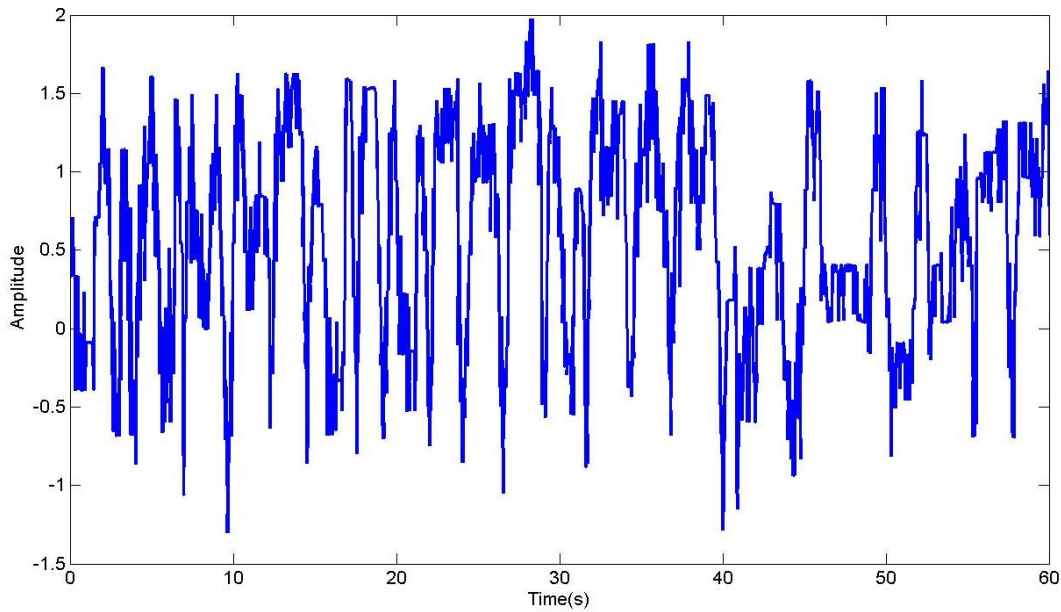


Figure 4-5 Result after applied Fourier Transform on pre-processed signal.

The continuous phase could be extracted by applying Fourier Transform on the pre-processed signal. By finding the coefficients from all samplers in each frame, the curve in Figure 4-5 could be obtained.

Assume the normal breath rate is in the range of 6 to 40 times per minute, a band-pass filter with bandwidth from 0.1 to 0.7 Hz is applied. Figure 4-6 shows the design view of the filter.

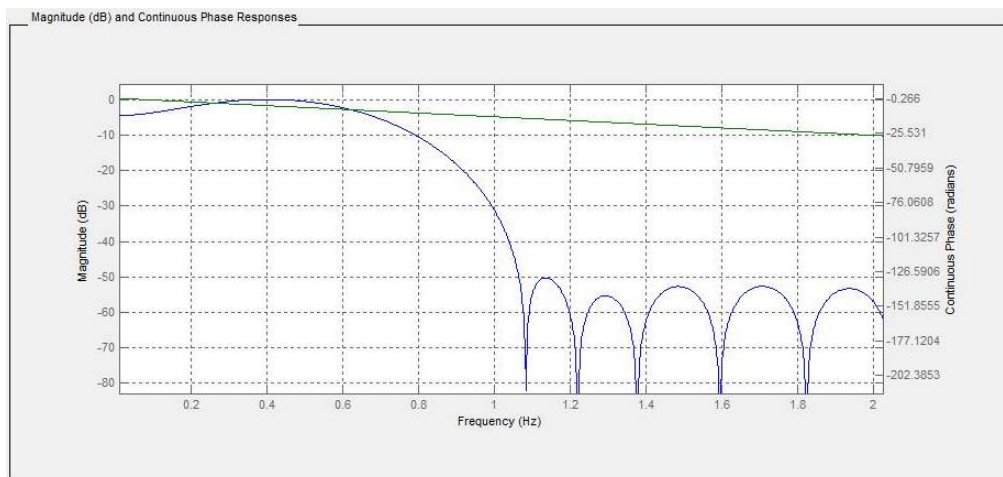


Figure 4-6 Design view of the band-pass filter.

4.2.4 Breath Signal Retrieval

In order to avoid counting small false peaks into the result, the peak counting procedure follows the algorithm below:

Calculate the mean value *mean* and the standard deviation *std* of the processed signal.

Set the possible range of the distance between two true peaks *min* and *max* based on the fact that breath frequency that we are interested in, which is from 0.1 to 0.7 Hz with the formulas below:

$$min = \frac{frameRate}{0.7} \quad (4.5)$$

$$max = \frac{frameRate}{0.1} \quad (4.6)$$

Find all peaks on the breath curve and save in a list *p*. Go through elements in *p* in order with following procedure:

- Create an empty vector *peaks* for breath peak storage;
- For each element *p_i*:
 - if** *p_i* > *mean* + *std* AND from last breath peak < *min*:
 - if** *p_i* < *p_{i-1}*, *p_i* is NOT a breath peak;
 - else** *p_{i-1}* is NOT a breath peak, *p_i* is a breath peak;
 - else if** *p_i* > *mean* + *std*, *p_i* is a breath peak;
 - else if** *mean* + *std* > *p_i* > *mean* AND from last breath peak ≥ *max*, *p_i* is a breath peak;
 - else** *p_i* is not a breath peak.

At the end, count the number of breath peaks.

4.3 Result and Discussion

Figure 4-7 shows the frequency domain of one sample among all measurements before and after the band pass filter, which are in black and blue, respectively. As shown in the figure, the signal with higher frequency has been sufficiently suppressed.

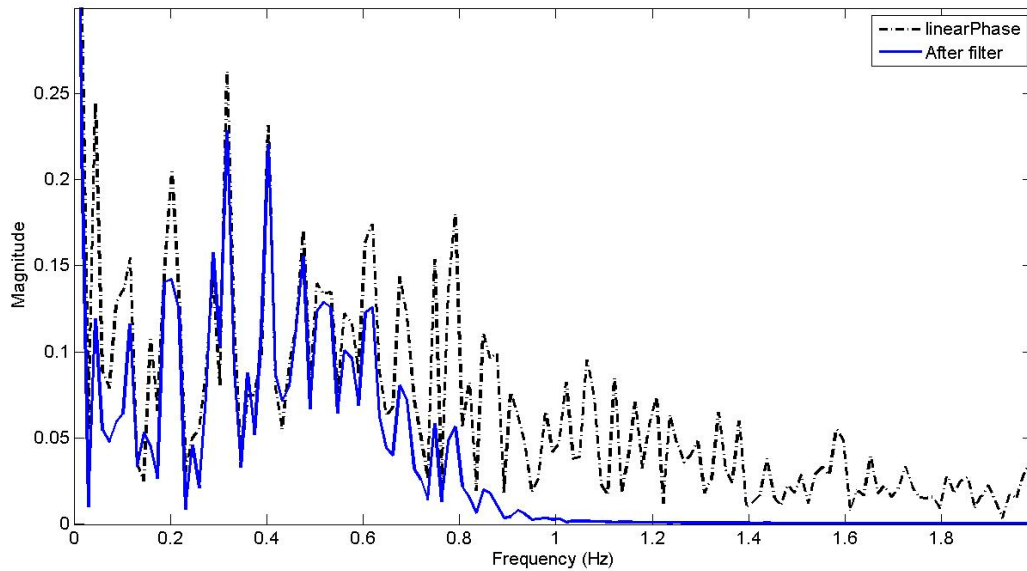


Figure 4-7 Signal before and after the band-pass filter in frequency domain.

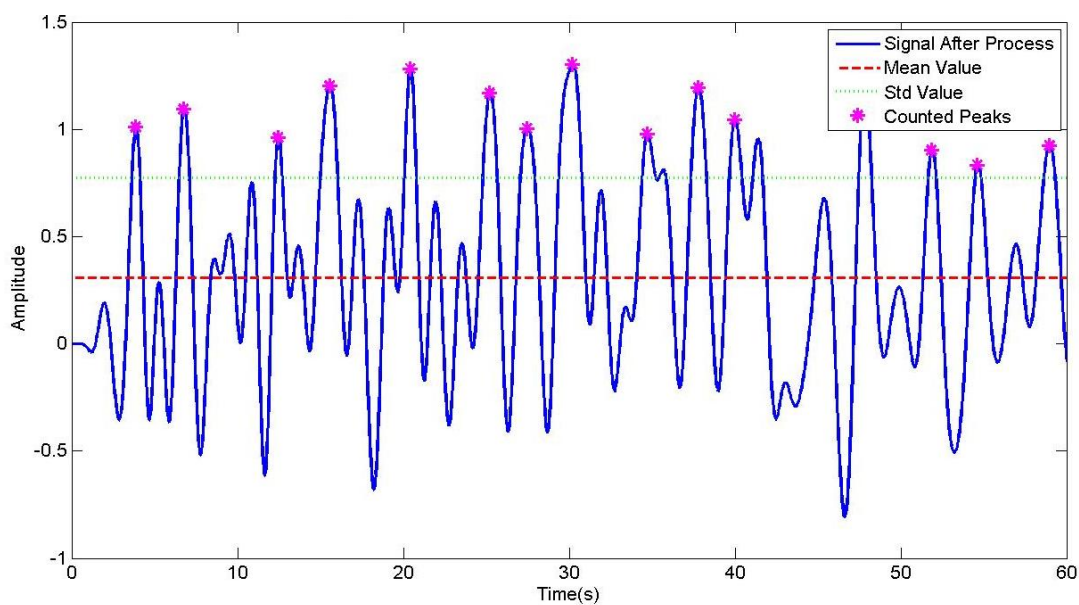


Figure 4-8 Result of a one minute sample after peak counting.

Figure 4-8 shows the final result from a one minute sample after peak counting. The blue curve indicated the signal, while the red and green lines are the mean value and the standard deviation value. The peaks with pink point are those we counted as a breath peak, which are 15 in total. The actual breath was 14 times during the measurement. The result is relatively good.

5 Heart Rate Detection

5.1 Computer Simulation

Before real experiment, a computer simulation has been done. Three methods were used to process the simulation signal, which were band-pass FIR1 filter, Empirical Mode Decomposition (EMD) and Wavelet packets.

5.1.1 System Modeling

We assume that despite, the signal from a still human contains information mainly about the breath and the heartbeat even though there are random noises and movements from other inner parts of human body, such as blood flow. Moreover, it is assume that the breath and the heartbeat of a human in a short period of time, such as one minute, remain stable with regular frequencies. Based on these assumptions, two sine waves with different amplitude and frequency were used to simulate human heartbeat (the black curve in the figure below) and breathe (the blue curve), respectively. In this model, the simulated heart rate is 90 times per minute (1.5 Hz) and the breath rate is 15 times per minute (0.25 Hz). A random number 0.956 is used as the initial phase difference. The composed signal (the red curve) from these two sine waves was used to simulate the measured signal. All three signals were generated by:

$$\text{heartBeat}(t) = 0.5 * \sin(2 * \pi * 1.5 * t) \tag{5.1}$$

$$\text{breath}(t) = 4 * \sin(2 * \pi * 0.25 * t + 0.956) \tag{5.2}$$

$$\text{composedSignal} = \text{heartBeat}(t) + \text{breath}(t) \tag{5.3}$$

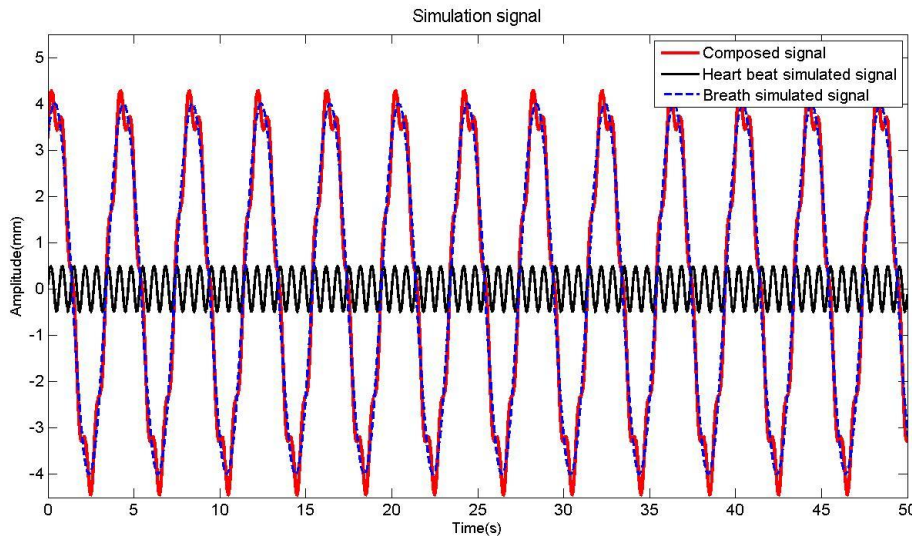


Figure 5-1 Heart rate simulation signal and its components.

Figure 5-2 shows the composed signal in the frequency domain. There are two large peaks that indicate the frequencies of breath and heartbeat, which are around 0.25 and 1.5 Hz respectively.

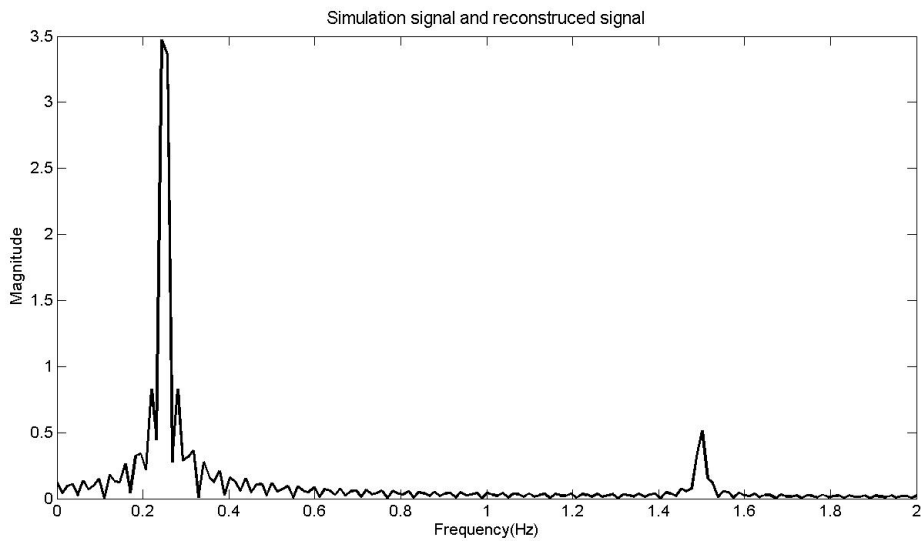


Figure 5-2 Simulation signal in frequency domain.

5.1.2 Methodology

5.1.2.1 Band-pass Filter

For this model, a FIR1 band-pass filter is naturally used for the first attempt to retrieve the heartbeat signal. Figure 5-3 shows the filtered signal in frequency domain. It can be seen that although the filter is able to depress the breath signal significantly, there is still a small peak at around 0.25 Hz, which indicate that might not be sufficient for this problem by using a single filter.

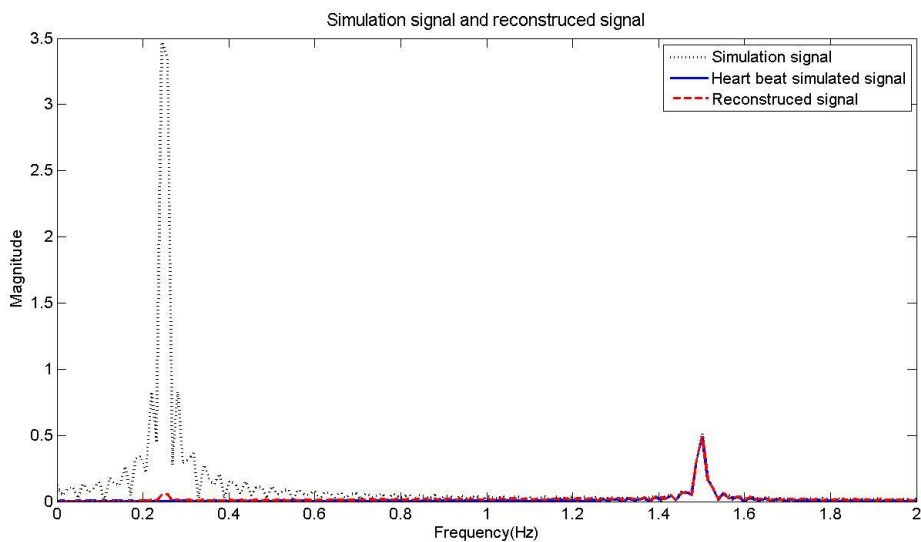


Figure 5-3 Simulated signals and reconstructed heart beat signal in frequency domain.

The figure below compares the processed signal and the original simulation signal. As we can see, the processed signal basically keeps the same shape with the original one, but with a little shift on the time and some amplitude differences on peaks.

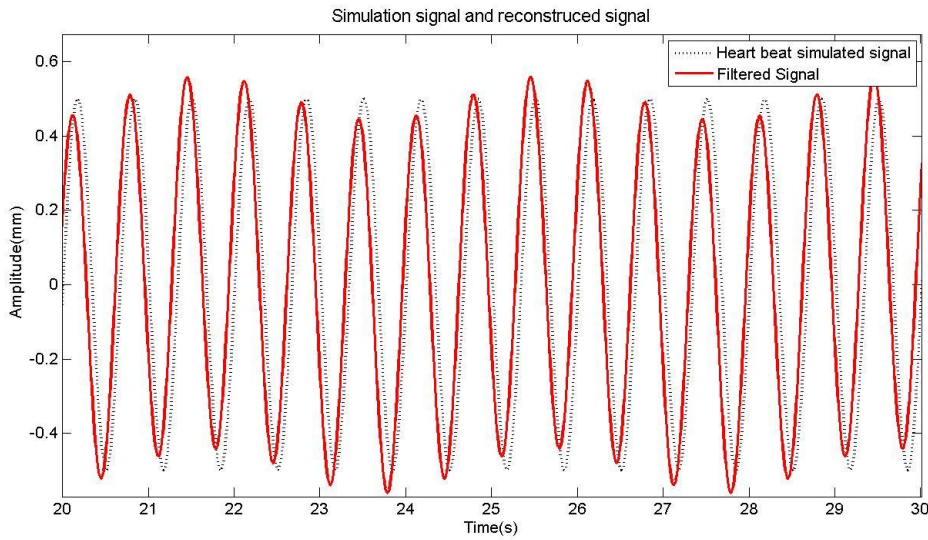


Figure 5-4 Simulated heart beat signal and the filtered reconstructed heart beat signal.

5.1.2.2 Empirical Mode Decomposition (EMD)

Empirical Mode Decomposition (EMD) is a nonlinear technique that can decompose a signal into finite components known as Instantaneous Mode Functions (IMF), which was developed by N.E. Huang in 1998. [13]

The algorithm works as below: for a signal $s(t)$, which is the black curve in Figure 5-5: [13]

- Find all minima and maxima extremes and plot a curve for each set by using cubic spline interpolation, which are the blue and red curves respectively.
- Compute the mean values between the maxima and minima curves, and make a residual curve $r(t)$ which is the pink one in the figure.
- Get the detail known as IMF by $d(t) = s(t) - m(t)$.
- Repeat the process above on the residual $r(t)$ until it fits the stopping criteria.

The stopping criteria can be defined based on the requirement of the analysis. In this thesis project, a existing library is used for calculation which defines the calculation stops once all condition below are satisfied:

- For each point, $\text{mean}_{\text{Amplitude}}(t) < 0.5 * \text{amplitude}(t)$;
- $\text{mean of } \text{bool}_{\text{criteria}}(t) \text{ less than } 0.05$;
- There are less than two extremes in the curve.

where

$$\text{mean}_{\text{Amplitude}}(t) = \text{abs} \left(\frac{\max_{\text{Amplitude}}(t) + \min_{\text{Amplitude}}(t)}{2} \right) \quad (5.4)$$

$$\text{amplitude}(t) = \text{abs}\left(\frac{\max_{\text{Amplitude}}(t) - \min_{\text{Amplitude}}(t)}{2}\right) \quad (5.5)$$

$$\text{bool}_{\text{criteria}}(t) = \left(\frac{\text{mean}_{\text{Amplitude}}(t)}{\text{amplitude}(t)}\right) > 0.05 \quad (5.6)$$

By this algorithm, the given signal is expected to be decomposed into several sub signals with different frequencies.

Figure 5-6 shows the outcome of the simulated signal by applying EMD. As showed in the figure below, the decompose procedure stops after the second iteration. The graph on the top is the composed simulation signal over 50 seconds time period. The two graphs below are the IMFs from the first and second iteration, which are referred as IMF1 and IMF2 respectively.

IMF1 is a sine-like wave with 75 peaks during 50 seconds (1.5 Hz) and average amplitude of about 0.5, which fit the original heartbeat simulation signal. IMF2 is also a sine-like wave, with 13 peaks during 50 seconds (0.26 Hz) and average amplitude of about 4. Considering the last peak is from an uncompleted cycle, it is reasonable to ignore the slightly difference between IMF2 and the original breath simulation signal. Therefore, both the heartbeat and breath signals are nicely retrieved by EMD.

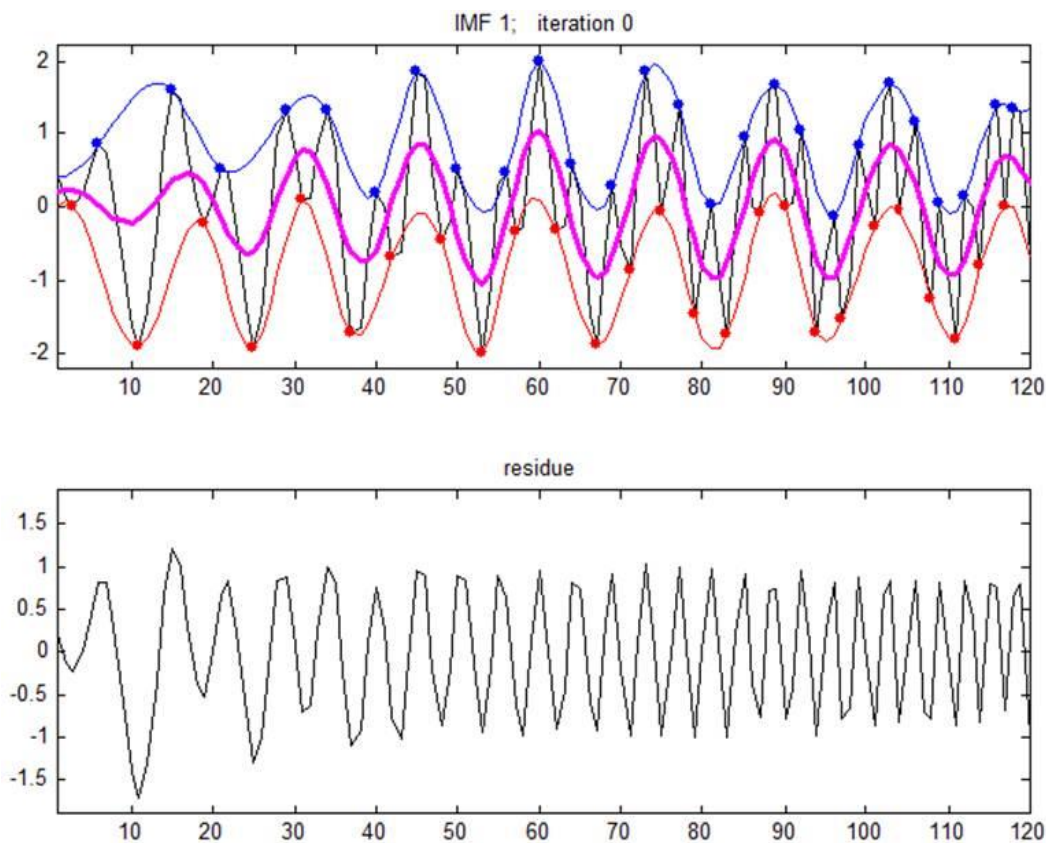


Figure 5-5 Signal and residue after the first iteration with EMD method.

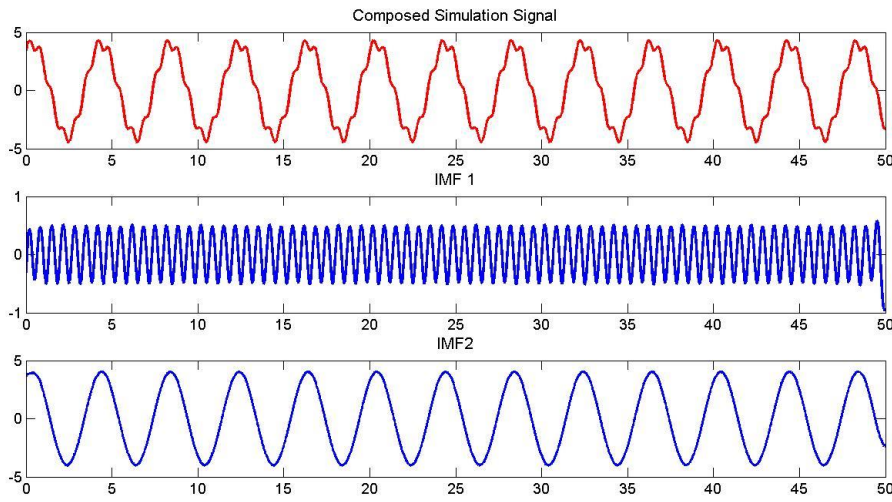


Figure 5-6 IMF1 and IMF2 of the composed simulation signal.

Figure 5-7 shows the composed signal, the heartbeat simulation and the IMF1 in frequency domain. It is clear that by using EMD, the signal in lower frequency range was suppressed sufficiently while the heartbeat signal was remain almost untouched.

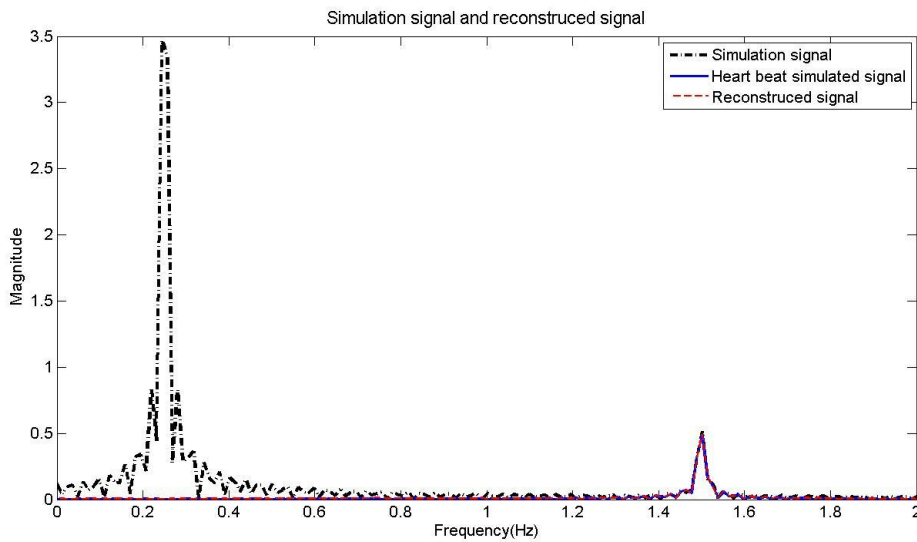


Figure 5-7 Simulated signals and reconstructed heart beat signal in frequency domain.

From comparing the simulation signal and IMF1 in time domain, it can be seen in Figure 5-8 that after applying the EMD method, the heartbeat signal could be nicely retrieved.

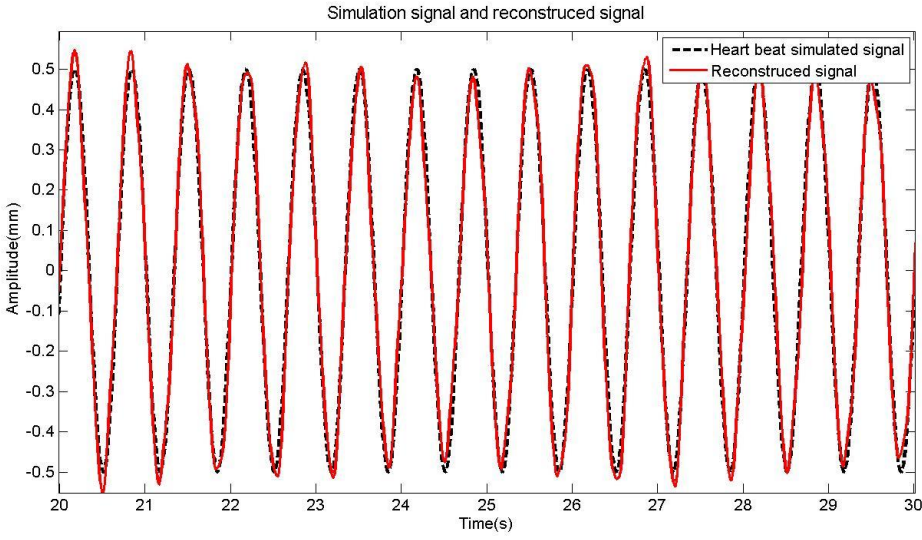


Figure 5-8 Simulated heart beat signal and the filtered reconstructed heart beat signal.

5.1.2.3 Wavelet Packets

Wavelet is a technique for decompose time series with different scales and times. [8] By using Wavelet transform, a signal could be divided into two parts: Signals in lower frequency (A, approximation coefficient) and higher frequency (D, details). By using wavelet packets, the Wavelet transform is first applied to the original signal and get A and D. Then the transform is applied again on both A and D and their outcome, respectively.

In other words, this analysis will produce a binary tree like in Figure 5-9. S is the original signal, which is the root node (0, 0) on the top of the tree. By applying wavelet transform on node (0, 0), signal could be decomposed into two parts, node (1, 0) and node (1, 1), which are the sub signal in lower frequency and the higher frequency respectively in level 1. The decompose procedure could continue with both nodes to get to the 2nd level of the tree with 4 nodes. Therefore, on the nth level, the tree should have 2ⁿ nodes. Considering the signal could be reconstruct from any node, this method could enable us to select the signal in the frequency that is interested in.

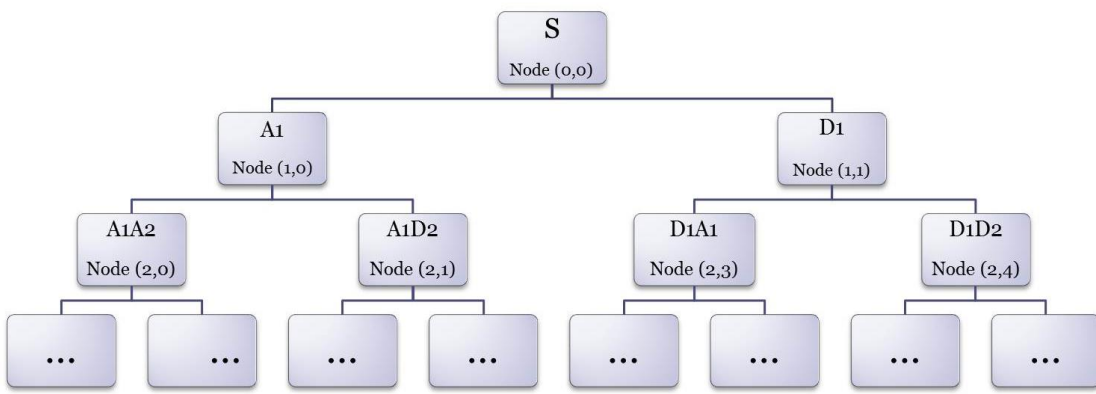


Figure 5-9 Binary tree produced by wavelet packets methods.

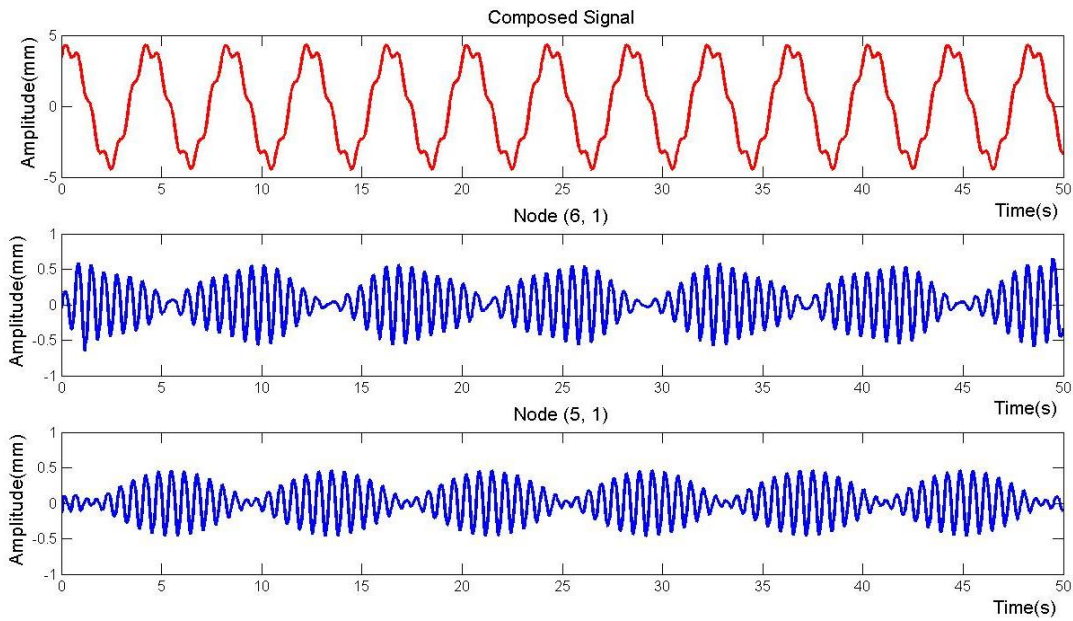


Figure 5-10 the composed simulation signal and two signals with target frequencies.

The red signal in Figure 5-10 is the composed simulation signal. The rest two blue curves are from the node (5, 1) and node (6, 1) with the target frequencies. The reconstruction signal was composed by these two signals.

From Figure 5-11 it can be seen clearly that the reconstructed signal perfectly fits the heartbeat simulation signal in the frequency domain and the breath signal is nicely removed from it.

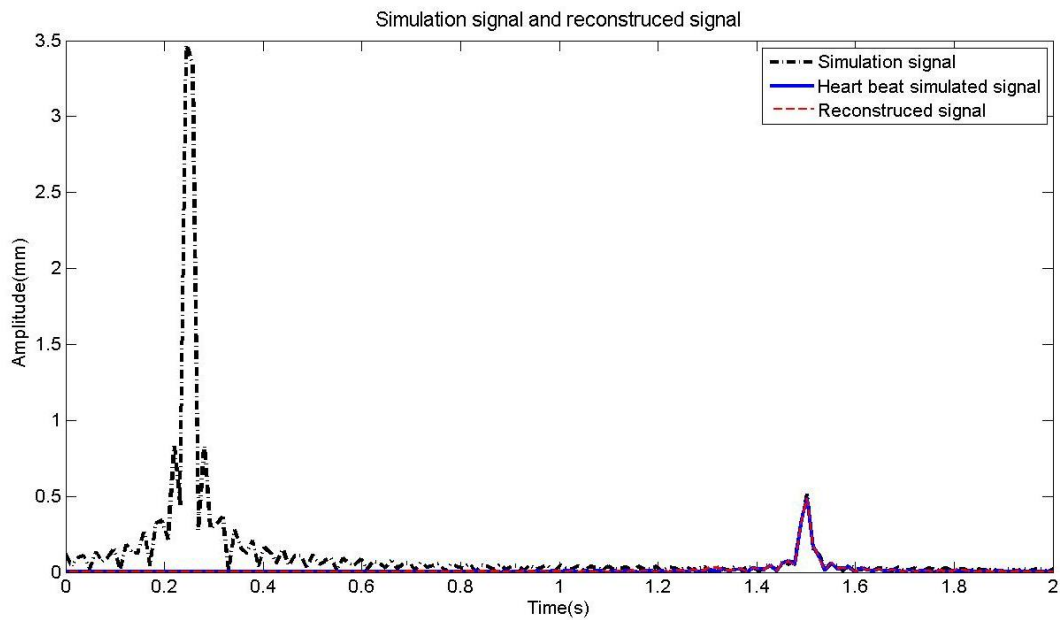


Figure 5-11 signals and reconstructed heart beat signal in frequency domain.

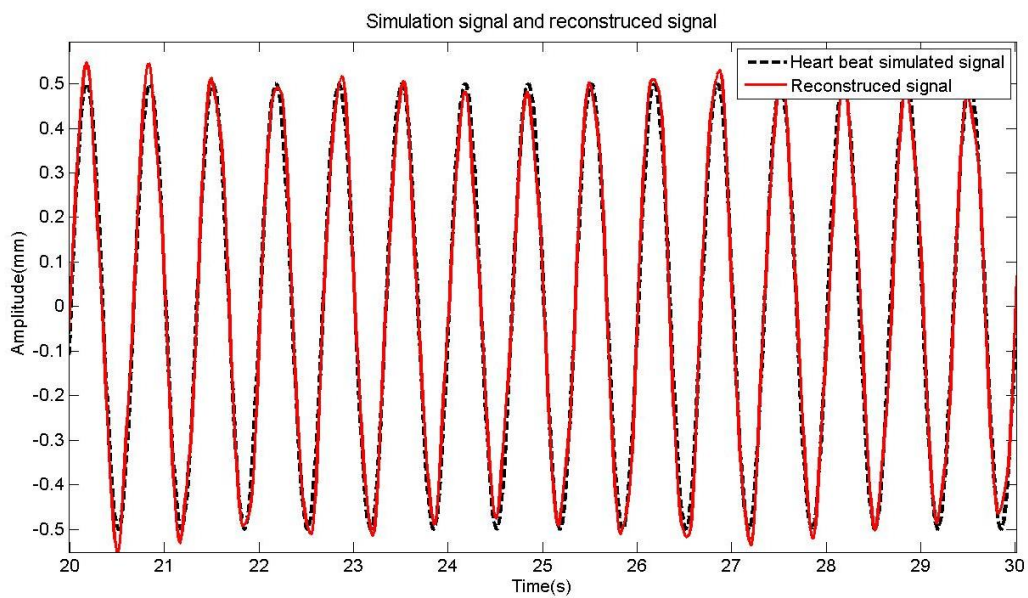


Figure 5-12 Simulated heart beat signal and the filtered reconstructed heart beat signal.

The red curve in Figure 5-12 is the reconstructed signal in time domain, composed by signals from the two nodes and the black curve is the simulation signal. It is obvious that the reconstruction signal basically fits the simulation signal with rather small errors.

5.2 Experiment with Corner Reflector

5.2.1 Measurement Setup

In order to quantify the detection capability of the radar system for small movements ($\pm 0.5\text{mm}$), such as human heartbeat, an experiment has been performed.

The experiment system contains following components:

- An Impo 1417 type function generator;
- An Impo 1419 type vibrator;
- A corner reflector(CR) which was made of three $6\text{cm} \times 6\text{cm} \times 6\text{cm}$ size boards with copper surface;
- The Novelda transceiver with two Vivaldi 004 antennas.

To rule out jamming from other sources, the measurement was performed in a magnetic shielded (MS) room. The whole test system except the desktop computer was placed inside the MS room. In Figure 5-13, the transceiver was hanged behind the wooden bracket, which could not be seen from this angle.



Figure 5-13 Photo of the experimental setup of corner reflector movement detection using the presented UWB radar system.

As shown in Figure 5-14, two Vivaldi 004 antennas were placed in parallel with 17cm distance. The vibrator and corner reflector were placed about 27cm from the outer edge of the antenna in vertical and right in the middle of two antennas. Therefore, the actual distance from the object to antennas is around 28cm.

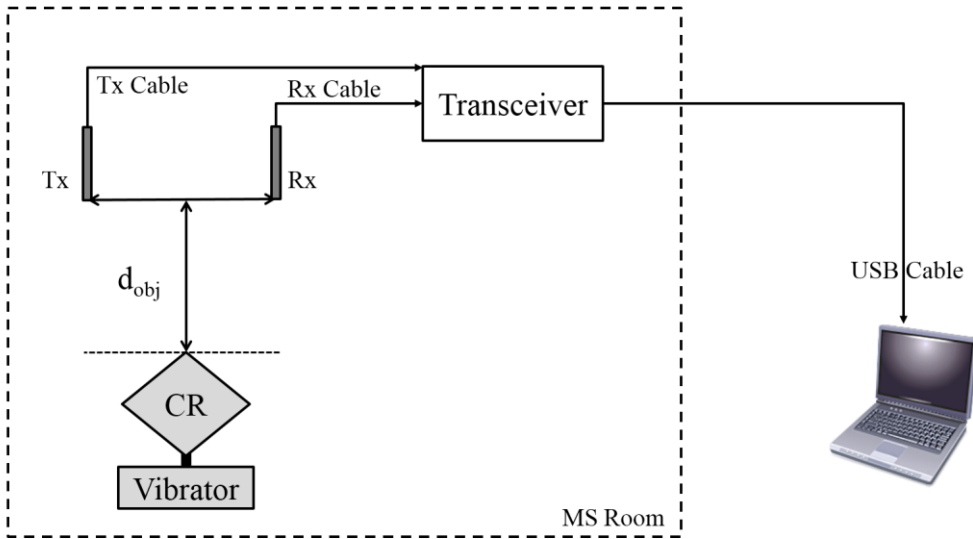


Figure 5-14 Diagram of the experimental setup of corner reflector movement detection using the presented UWB radar system.

Samples were taken with parameters in Table 4. Both the signal and the detection time were saved as matrix and vectors respectively.

Table 5 Experiment parameters.

Measuring Time	d_{obj}	d_a	CR movement	Excitation Frequency	Excitation Waveform
$\approx 60s$	$\approx 27cm$	$\approx 17cm$	$\pm 0.5mm$	1, 1.5, 2, 2.5, 3, 3.5 Hz	Sine, Triangular

5.2.2 Signal Processing

The signal processing procedure followed the diagram in Figure 5-15. All three methods, SVD, EMD and Wavelet Packets, are applied to the experimental signals separately. After signal has been processed, a peak counting method is applied to get the final result. In order to avoid counting small false peaks into the result, the peak counting method is designed like below:

- Calculate the mean value (mean) and the standard deviation (std) of the processed signal.
- Apply the threshold below to the signal:

$$f(sig) = \begin{cases} \text{mean} - \text{std}, & sig < \text{mean} \\ \text{mean} + \text{std}, & sig \geq \text{mean} \end{cases}$$

- Count the number of points in the signal after threshold that fit the condition: $f(s) = \text{mean} - \text{std}$ AND $f(s + 1) = \text{mean} + \text{std}$.

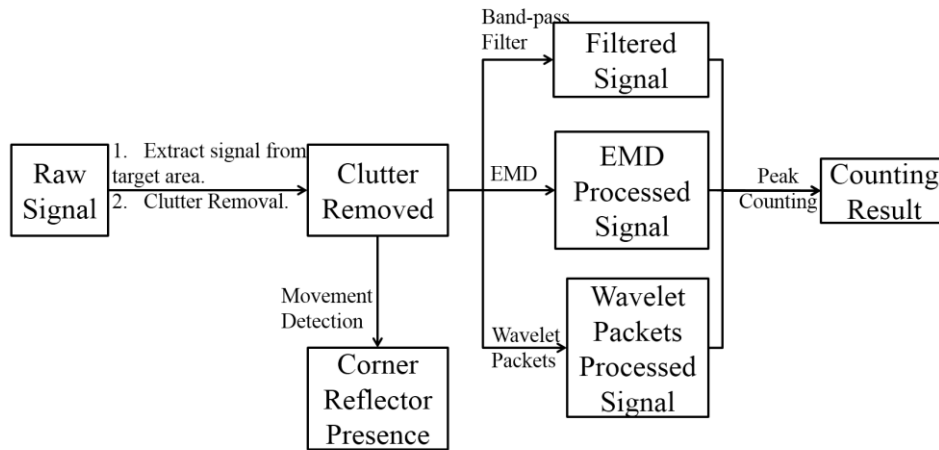


Figure 5-15 Signal processing procedure diagram for corner reflector movement detection.

5.2.3 Result and Discussion

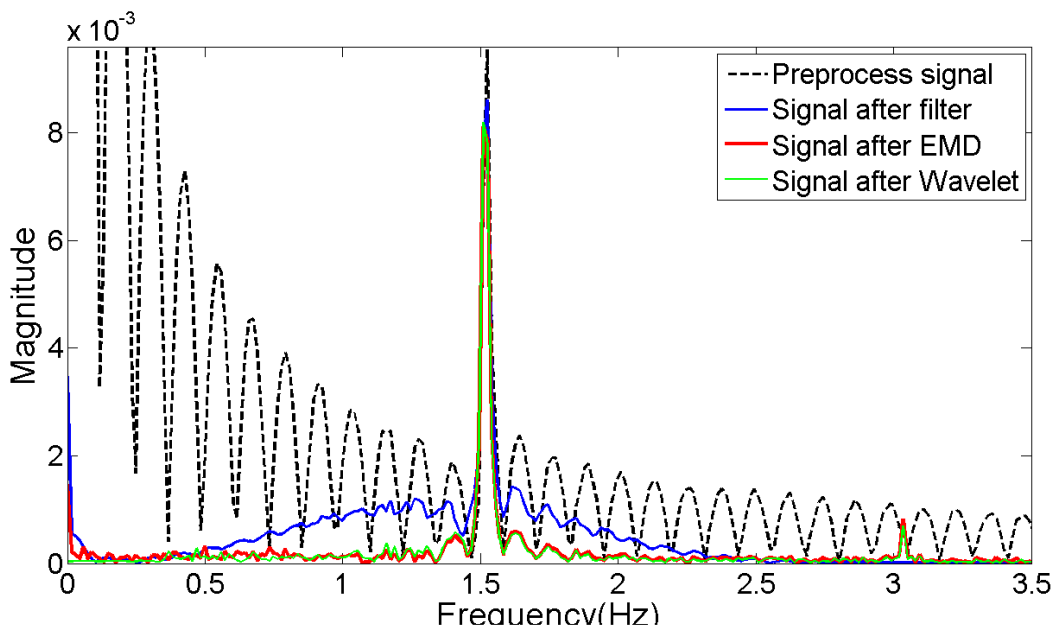


Figure 5-16 the results of signal of one sample with 1.5 Hz movement processed in the frequency domain.

Figure 5-16 shows the result in the frequency domain. The black curve is the preprocessed signal. The signal after the filter, EMD and Wavelet packets are in blue, red and green. It is obvious that the signal after filter contains relatively more signal around the target frequency. Considering in reality, the breath signal is much stronger than heartbeat signal and their main frequency are very close, the FIR1 band-pass filter method can hardly work.

All three methods have the same result of 91 beats for one minute (1.52Hz). This is quite close to the simulation frequency 1.5 Hz, which should be 90 beats ideally. However, the EMD has a relatively large error on signal amplitude as shown in Figure 5-17, which might be caused by frequency leakage. Frequency leakage here refers the phenomenon that IMF contains the signal which does not belong to its fundamental frequency. This could be caused by several reasons. One of them is that the mean values are calculated by interpolation values based on the minima and maxima extremes sets, which means they are not the true mean values. Moreover, in each iteration, the IMF is only a partial signal from the original one that is highly effected by the calculated mean values. Therefore, all approximations in the calculation make frequency leakage unavoidable in EMD method.^[17] Besides that, due to the difficulty to pre-determine the fundamental frequency of each IMF, the reconstruction work could be tricky because it is hard to predict which IMF should be included into the result.

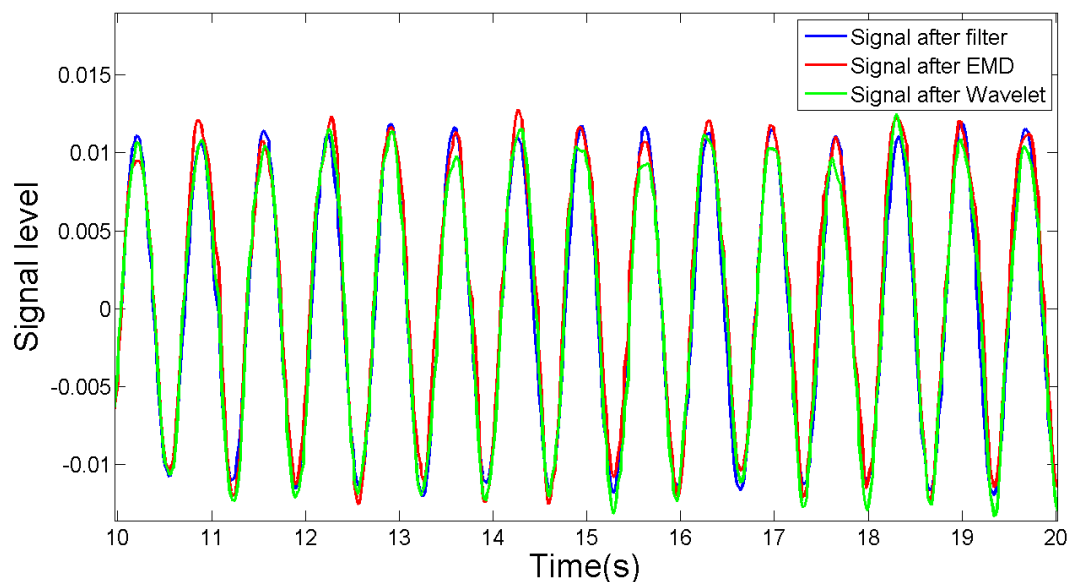


Figure 5-17 Results of different processing method applied on the experiment signal.

5.3 Measurement with Real Human

The measurement setup remained the same with the breath detection. The raw signal was processed with following procedure shown in Figure 5-18.

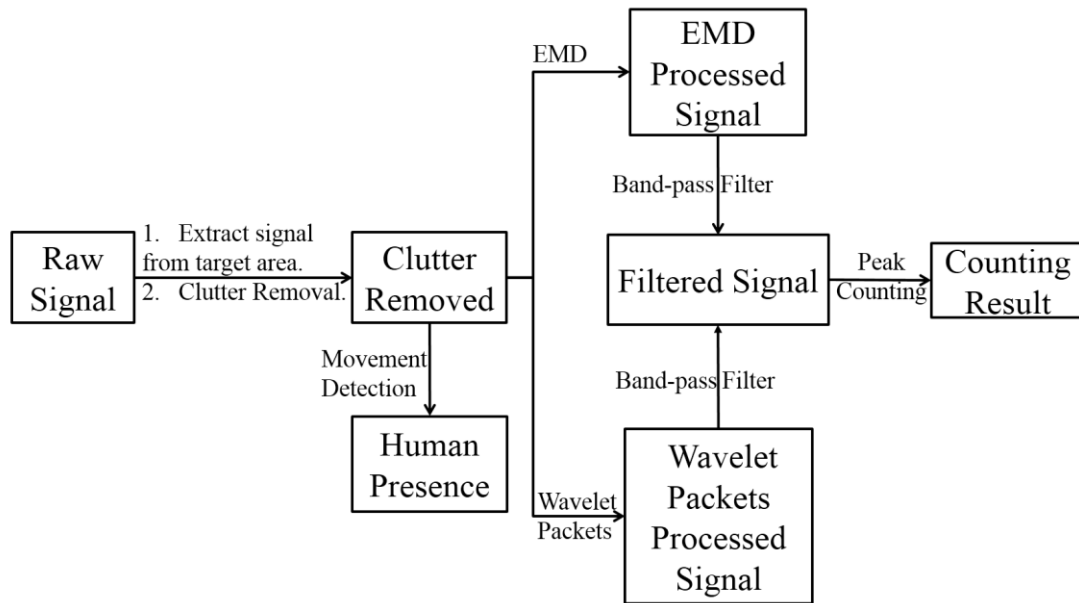


Figure 5-18 Signal processing procedure diagram for heartbeat detection

5.3.1 Motion Detection

Figure 5-19 shows the motion detection result from a one-minute sample with 78 times heartbeat. With the presence of a human, the peak raised from around 700 to 2300. This indicated that a strong periodic signal is obtained.

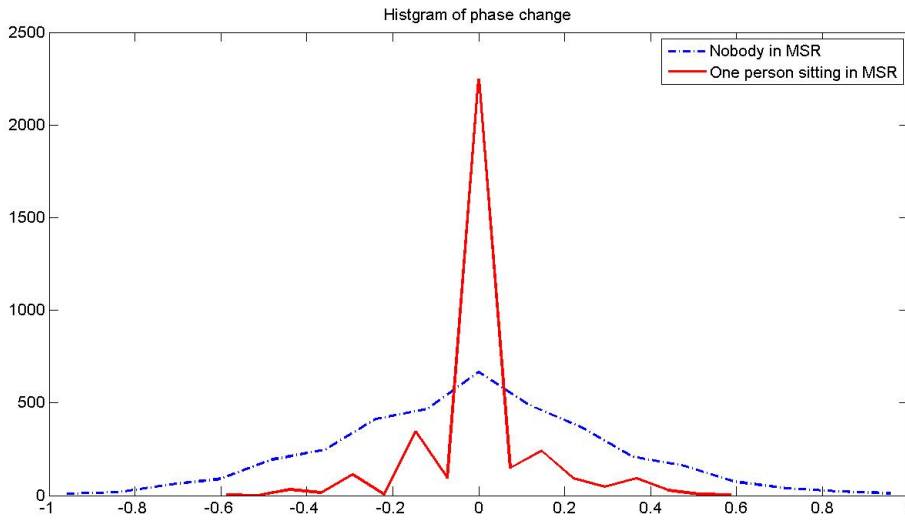


Figure 5-19 Motion detection result of one sample with one human sitting in the radar range.

5.3.2 EMD

In the Figure 5-20, the red curve is the preprocessed signal. Following four curves are the signals from IMF 3, 4, 5 and 6 that are used to reconstruct the signal, which is the curve at the bottom.

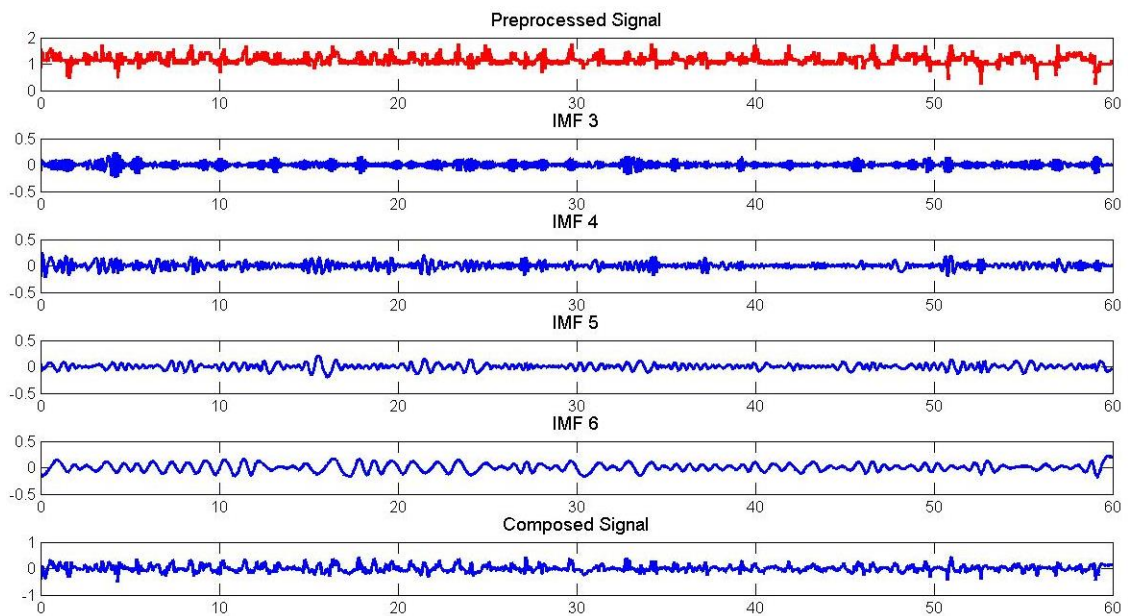


Figure 5-20 IMFs produced by applying EMD on pre-processed signal and the signal composed by them.

The outcome after filtering is shown in Figure 5-21. There are 75 beats counted from the processed signal, which has 3 beats missing. By using a simulation sine wave with frequency 1.2 Hz as a reference, it shows that some very small peaks were seen as one peak with other peaks.

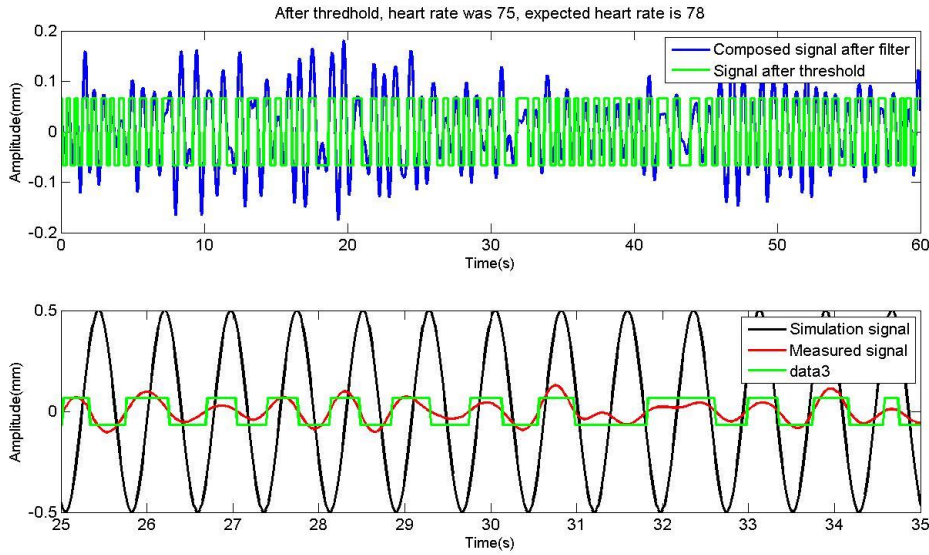


Figure 5-21 the reconstructed signal after filtering and peak counting.

5.3.3 Wavelet Packets

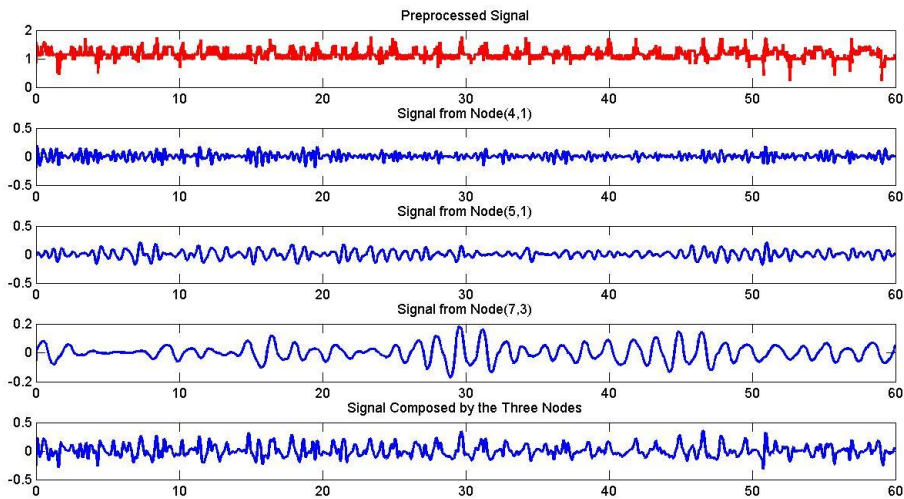


Figure 5-22 Signals from different nodes that are produced by applying wavelet packet on pre-processed signal and the signal composed by them.

In the Figure 5-22, the red curve is the preprocessed signal. Following three curves are the signals from node (4, 1), (5, 1), and (7, 1) that are in the human heart rate frequency range, which is from around 0.7 to 3.75 Hz. The curve at bottom is the composed signal from the three nodes, which is sent to the filter before peak counting.

The outcome after filtering is shown in Figure 5-23. There are 77 beats counted from the processed signal, which is very close to the real heartbeat 78 times. By using a simulation sine wave with frequency 1.2 Hz as a reference, it shows that the reconstructed signal basically match the shape of the simulation.

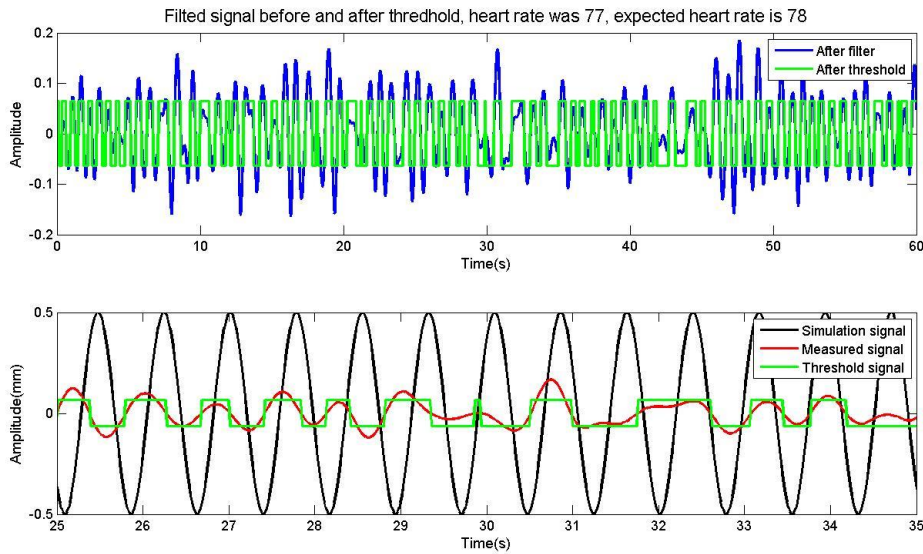


Figure 5-23 the reconstructed signal after filtering and peak counting.

5.3.4 Result and Discussion

Figure 5-24 shows the results in frequency domain. The black curve is from the preprocessed signal and the blue and red are from the results after EMD and Wavelet Packets. It is clear that the preprocessed signal contains many large peaks in the frequency range from 0 to 1 Hz, which mainly came from the breath. By applying EMD and Wavelet packets methods, not only signal in this range has been sufficiently depressed, but also the signal in higher frequency. As we can see from the figure, main peaks after process concentrate in the range 1.1 to 1.4 Hz. Considering the frequency spectrum has overall information of the sample for one minute and the real heartbeat is with around 1.2 Hz frequency, the results are relatively good.

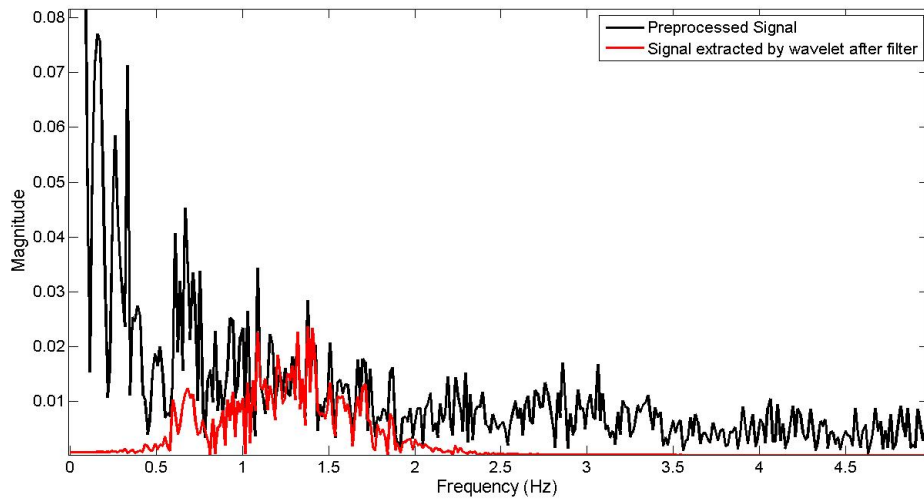


Figure 5-24 Pre-processed signal and the signal extracted by wavelet after filter in frequency domain.

Figure 5-25 shows the reconstruction result in time domain. Considering two curves share high similarity on their shapes and the number of peaks, it should be able to say that the heartbeat signal from a real human could be obtained by the radar system and be extracted with different signal processing methods.

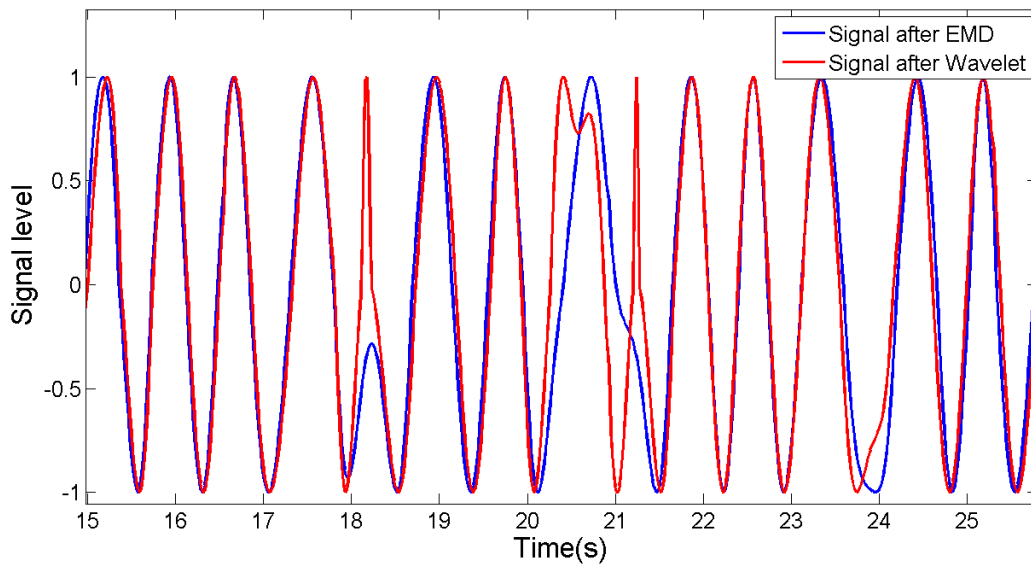


Figure 5-25 the heartbeats are reconstructed by sinusoid signals. This figure shows the normalized reconstructions from continuous measurements. The accuracy is evaluated by comparing the number of real heartbeats and reconstruction peaks.

6 Sand Flow Detection

Another interesting attempt of UWB radar application is sand flow detection. In icy winter days, sand is widely used for increasing the friction between the road surface and wheels. Trams normally carry a sandbox that can provide the sand in need. However, because the sand is pumped under the tram, the driver cannot really know if the sand has actually been pumping out. Therefore, it would be very interesting if a UWB radar application could do the monitoring work.

6.1 Experiment with Funnel

The main idea of the application is to see if the UWB radar can detect the sand flow in the range. In order to get rid of the noise of complex environment, which is the tram in this case, an experiment is done.

6.1.1 System Setup and Measurement Methodology

Two kinds of measurements were performed for trying to detect the reflection and transmission of the sand flow.

Figure 6-1 shows the diagram of the transmission detection experiment. Two Vivaldi 004 antennas are placed at both sides of the sand flow with the distance $d_{obj} = 54$ cm. The distance between antennas and the bottom of the funnel $h = 7$ cm.

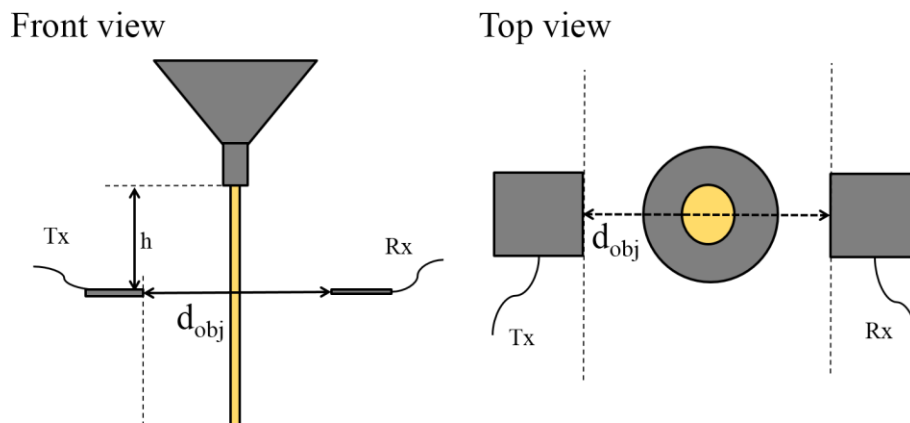


Figure 6-1 the diagram of the experimental setup for detecting the transmission of the sand flow. Graph on the left hand side shows the setup from the front view and the one on the right hand side shows from the top view.

Figure 6-2 shows the diagram of the reflection detection experiment. Two Vivaldi 004 antennas are placed at the same side with the distance $d_a = 10$ cm in between. Both of them face to the sand flow with the distance from the outer edge $d_{obj} = 25$ cm. The distance between antennas and the bottom of the funnel $h = 8$ cm.

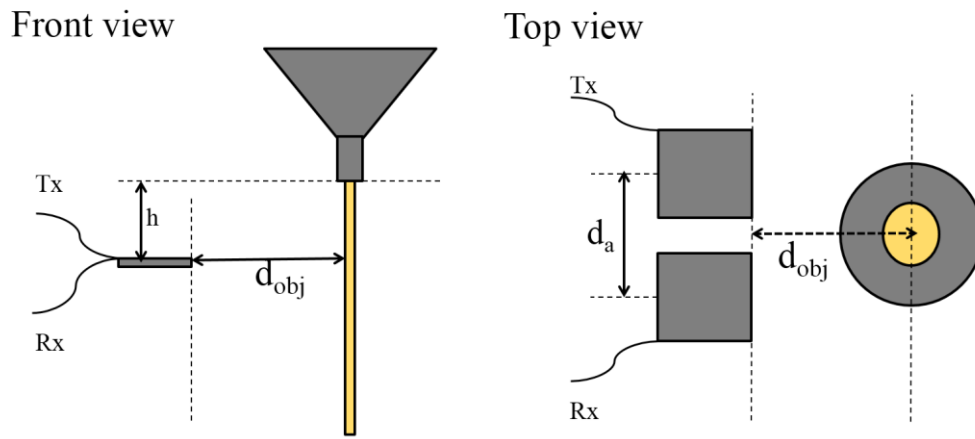


Figure 6-2 the diagram of the experimental setup for detecting the reflection of the sand flow. Graph on the left hand side shows the setup from the front view and the one on the right hand side shows from the top view.

6.1.2 Results and Discussion

The result in transmission detection is shown in Figure 6-3. The blue line is the mean value of all frames that collected with no sand flow. The red line is the mean value of all frames that measured with sand falls out of the sand by gravity. It can be seen clearly that the signal strength is reduced when the sand flow is passing the radar's range.

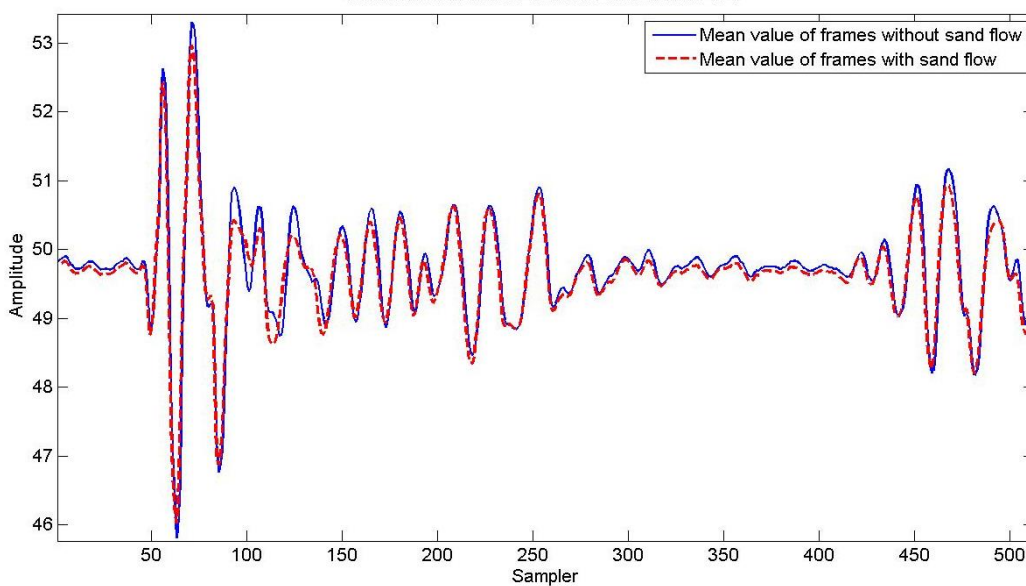


Figure 6-3 Measurement results for transmission detection of the sand flow.

The result in reflection detection is shown in Figure 6-4. The blue line is the mean value of all frames that collected with no sand flow. The red line is the mean value of all frames that measured with sand falling. As we can see, there is hardly any difference between these two signals, which indicate the sand flow has almost no reflection at all.

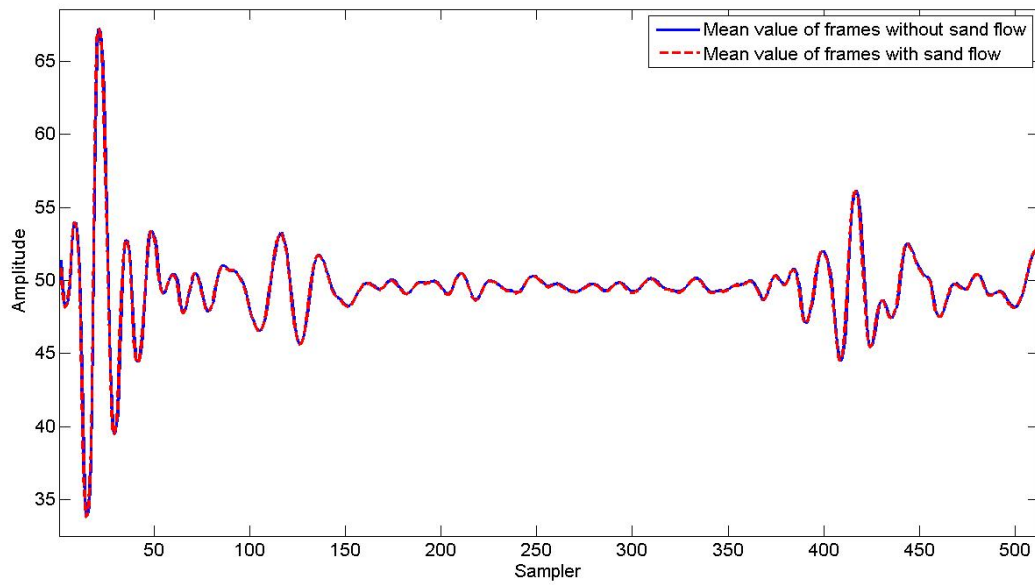


Figure 6-4 Measurement results for reflection detection of the sand flow.

This phenomenon could be explained by the form of the sand flow. Unlike metal plate, which has a flat surface that could reflect the incident waves directly back to the source, the sand flow scatters the incidences to arbitrary directions, and therefore the detectable reflections are not visible to the radar system.

6.2 Measurement with Sand Box

6.2.1 System Setup and Measurement Methodology

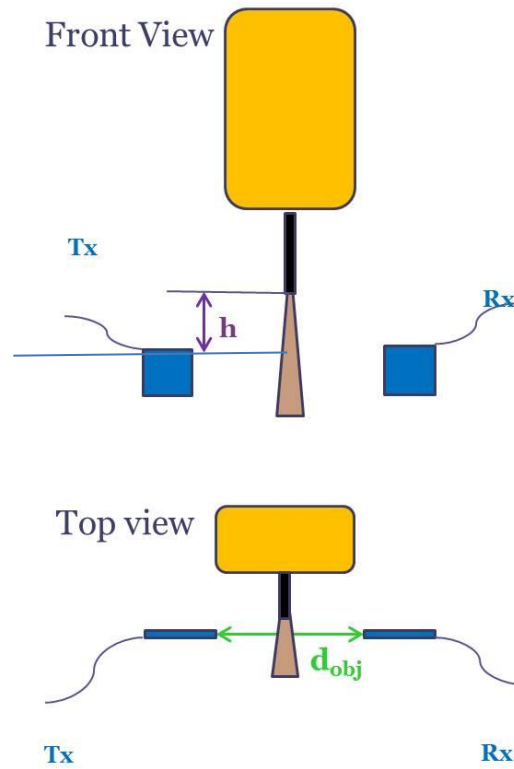


Figure 6-5 the diagram of the experimental setup for detecting the transmission of the sand flow from a real sand box. Graph on the top shows the setup from the front view and the one on the bottom shows from the top view.

Considering the transmission measurement has a better result in the previous experiment, it is used to measure the real sandbox that is used on trams. Figure 6-5 shows the diagram of the experiment system. Two Vivaldi 004 antennas are placed at both side of the sand flow with the distance $d_{obj} = 17.5$ cm. The distance between antennas and the bottom of the funnel $h = 7$ cm.

6.2.2 Result and Discussion

The result of the measurement is shown in Figure 6-6. The blue and the red lines are the mean value of all frames that collected without and with sand flow respectively. It can be seen that, unlike in the previous experiment, two curves are almost overlapped and it is hardly to see any difference.

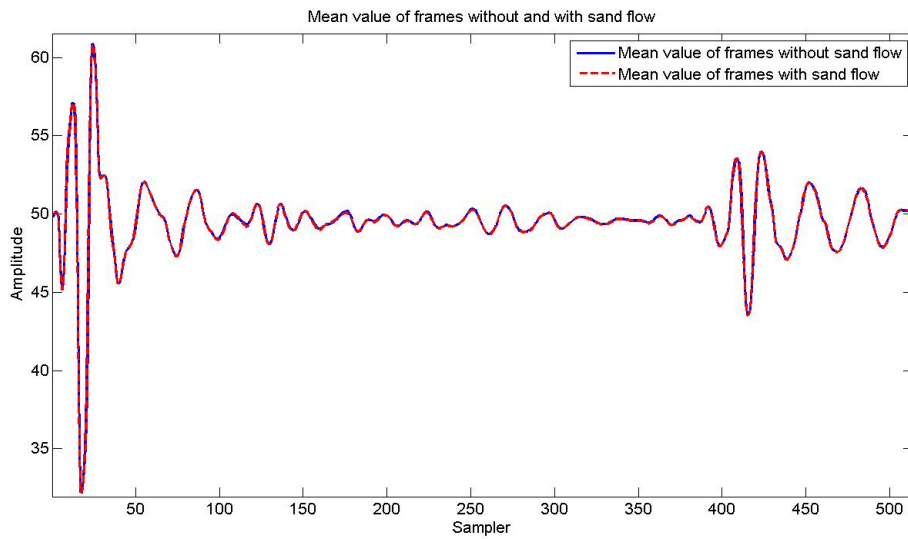


Figure 6-6 Measurement results for transmission detection of the sand flow.

This result can be explained by the difference between the density of the sand flow in the experiment and the sand flow generated by the sand box. In the experiment, the funnel has a 1 cm diameter hole at the bottom. The sand flow drops from the funnel has much higher density than the one blow out by the sandbox. Therefore, both reflection and transmission can hardly show any significant difference. In conclusion, the Novelda UWB radar system might not be able to provide a satisfied solution to this problem.

7 Summary and Future Work

Through this thesis work, several UWB radar applications are investigated and the corresponding signal processing algorithms are developed with good results, and one application (sand flow detection) is still open to good solutions. The summary is as follows:

- The breath detection has very stable performance that can work right in front of a human, and has a potential to work through a wall.
- The radar system is able to detect small movements, such as the movement in the experiment with $\pm 0.5\text{mm}$. The wavelet packets and EMD methods are shown to be very helpful in heart rate detection with suppressing breath interference, though the detection is sensitive to irregularly body movement.
- The radar system has been shown to have a high resolution in distance. It can track a quick moving object in the close range that have a relatively strong reflection.
- The radar system can detect a substance that has a strong reflection or can absorb the incident wave significantly.
- We have not yet found a good solution to detect the low density sand flow that generated by the sand box, due to the low reflection and high transmission.

A future work could be done with two or three radar modules at the same time, which could enable a two dimensions or even three dimensions resolution. Therefore, by using the correlation between the signals from different radar modules, a higher signal to noise ratio could be obtained. Besides that, more application might be investigated, such as multi-dimensions positioning, tracking, target recognition.

8 References

- [1] Ultra-wideband Transmission Systems, Federal Communications Commission, federal register, title 47, vol.1, 2002.
- [2] Ian Oppermann, Matti Hamalainen, Jari Linatti, *UWB Theory and Applications*, Wiley.com, 2006.
- [3] Ben Allen, Mischa Dohler, Ernest Okon, Wasim Malik, Anthony Brown, David Edwards, *Ultra Wideband Antennas and Propagation for Communications, Radar & Imaging*, Wiley.com, 2006.
- [4] Yinan Yu, Jian Yang, Tomas McKelvey and Borys Stoew, “A Compact UWB Indoor and Through-Wall Radar with Precise Ranging and Tracking”, *International Journal on Antenna and Propagations*, vol. 2012, Article ID 678590, 11 pages, 2012.
- [5] J. Yang and A. Kishk, “A novel low-profile compact directional ultra-wideband antenna: the self-grounded Bow-Tie antenna”, *IEEE Trans. on Antennas Propag.*, vol. 60, no. 3, pp. 1214-1220, March 2012.
- [6] J. Yang and A. Kishk, “The self-grounded Bow-Tie antenna”, *2011 IEEE international Symp. on Antennas Propag.*, Spokane, Washington, USA, July 3-8, 2011.
- [7] S.Fayazi, H.-S. Lui and J. Yang, “Microwave Imaging of Near-Field Object Using Ultra-Wideband Synthetic Aperture Radar Algorithm”, *2012 IEEE international Symp. on Antennas Propag.*, Chicago, IL, USA, July 8-14, 2012.
- [8] A-Rawi, Jian Yang, Charlie Orlenius and Magnus Franzen, “The Double-sided 4-port Bow-tie antenna: A new compact wideband MIMO antenna”, *7th Eur. Conf. on Antennas Propagat. (EuCAP2013)*, Gothenburg, 8-12 April 2013.
- [9] Fayazi, Jian Yang, Hoi-Shun Lui, “UWB SAR imaging of near-field object for industrial process applications”, *7th Eur. Conf. on Antennas Propagat. (EuCAP2013)*, Gothenburg, 8-12 April 2013.
- [10] Shirin Abtahi, Jian Yang, and Stefan Kidborg, “A new compact multiband antenna for stroke diagnosis system over 0.5-3 GHz”, *Microwave and Optical Technology Lett.*, Vol. 54, No. 10, pp. 2342–2346, October 2012.
- [11] Vivaldi 006 Anti-podal directional antenna, Imego AB
- [12] Vivaldi 004 Directional antenna, Imego AB
- [13] Gabriel Rilling, Patrick Flandrin, Paulo Goncalves, “On Empirical Mode Decomposition and its Algorithms”, *IEEE-EURASIP Workshop on Nonlinear Signal and Image Processing NSIP*, vol. 3, pp. 8-11, 2003.
- [14] Donald B. Percival and Andrew T. Walden, *Wavelet Methods for Time Series Analysis*, vol. 4, Cambridge University Press, 2006.
- [15] <http://www.novelda.no>, Novelda AS
- [16] NVA6100 Preliminary Datasheet, Impulse Radar Transceiver System, Novelda AS
- [17] N.E. Huang, Z. Shen, S.R. Long, M.L. Wu, H.H. Shih, Q. Zheng, N.C. Yen, C.C. Tung and H.H. Liu, “The empirical mode decomposition and Hilbert spectrum for nonlinear and non-stationary time series analysis,” *Proc. Roy. Soc. London A*, Vol. 454, pp. 903–995, 1998

9 Appendix A: Demo system

In order to demonstrate the possible applications the radar system could be used in, a demo system has been made. The system is based on the APIs offered by Novelda for the radar system. The GUI and signal processing algorithms are written with Matlab.

9.1 Raw Data

Show the unprocessed raw data from the radar system in the frame view.

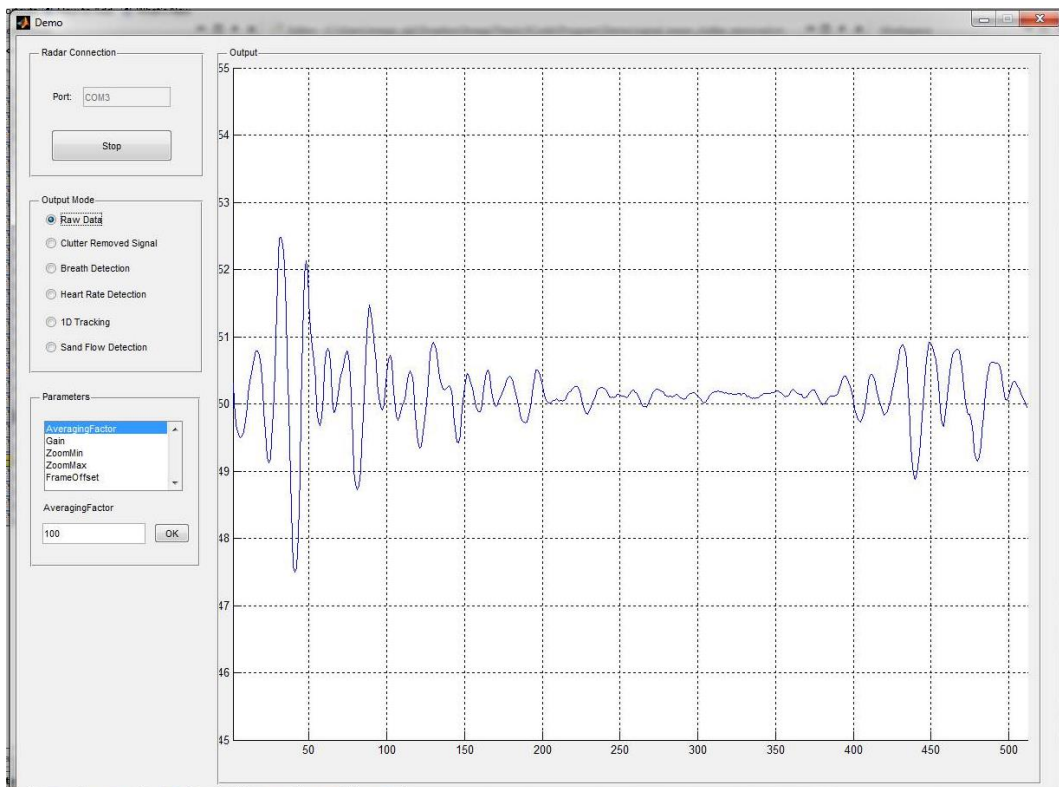


Figure 9-1 Screen shot of raw signal from radar.

9.2 Clutter Removal

Show the clutter removed signal with SVD method in the frame view. [4]

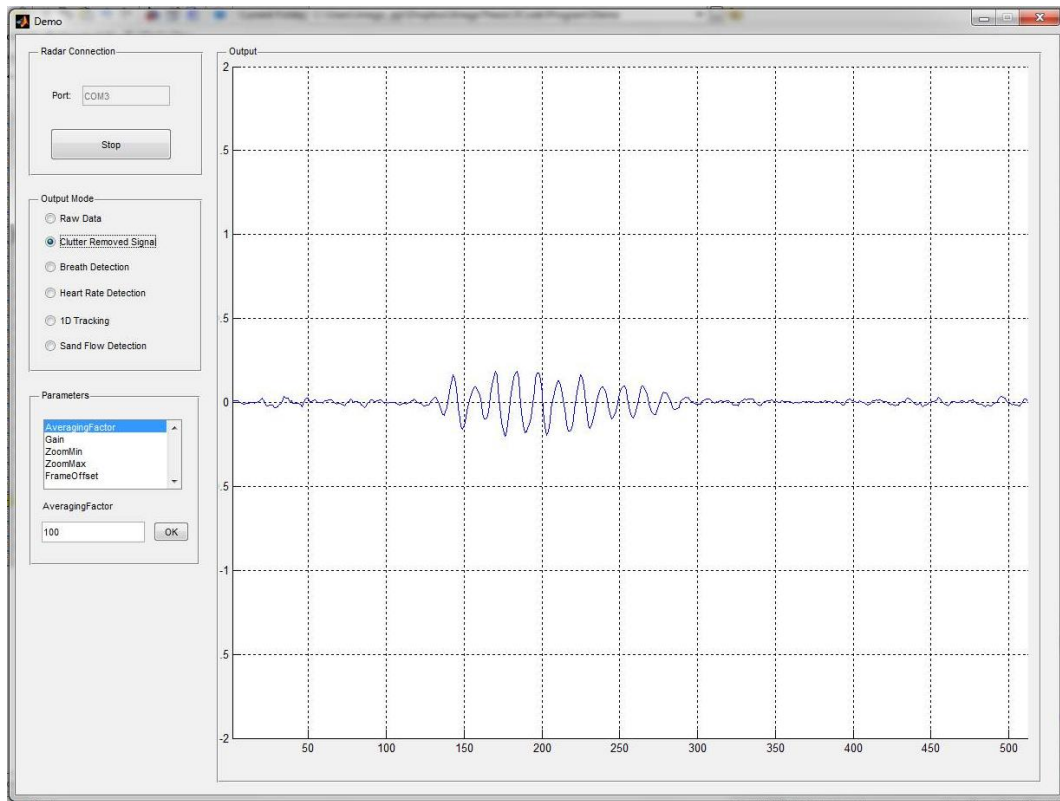


Figure 9-2 Screen shot of a clutter removed signal.

9.3 One Dimension Tracking

A function based on the previous work [4], which achieved one dimensional tracking by using Kalman filter.

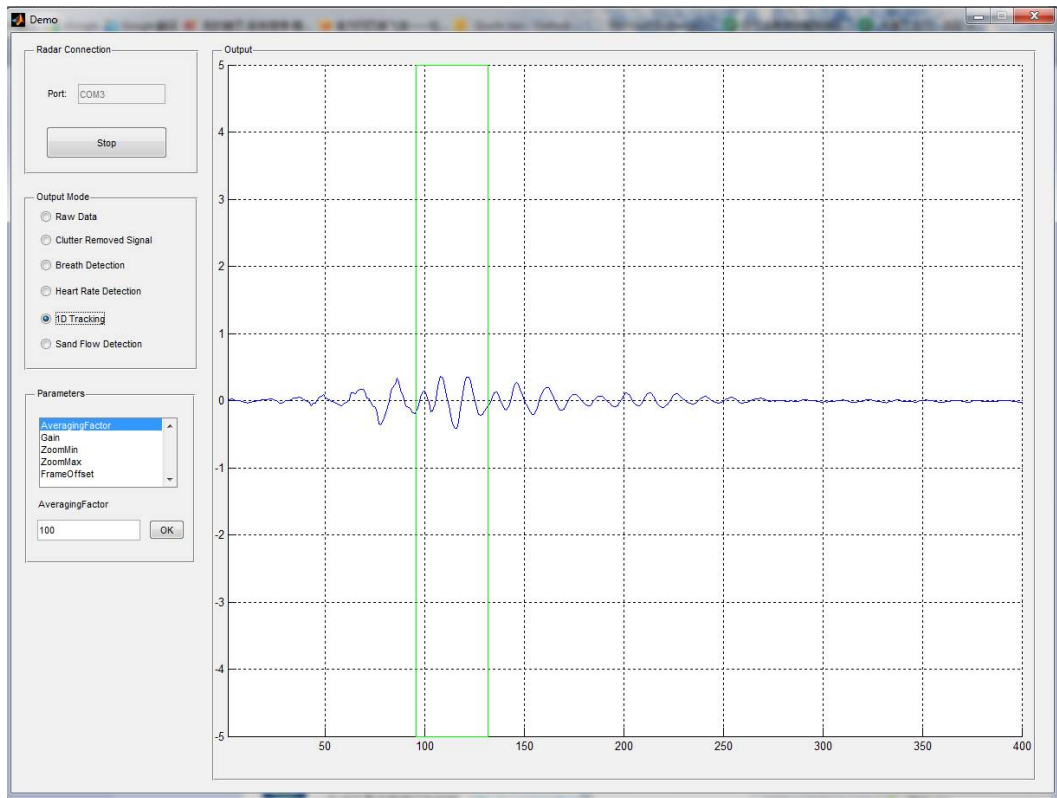


Figure 9-3 Screen shot during one dimension tracking on a moving metal board in the radar range.

9.4 Breath Detection

A function variant from the off line breathes detection method. The function provides the real time breath rate by following procedure:

- Collect signal until the data matrix reach certain size;
- Start the loop below until the system quit this function:
 1. Update the breath rate in every n seconds(where n is adjustable) by following steps:
 - Calculate the frame rate and other key value for further processing;
 - Detect breath rate;
 2. Drop the oldest signal and put the new signal at the end of the data matrix.

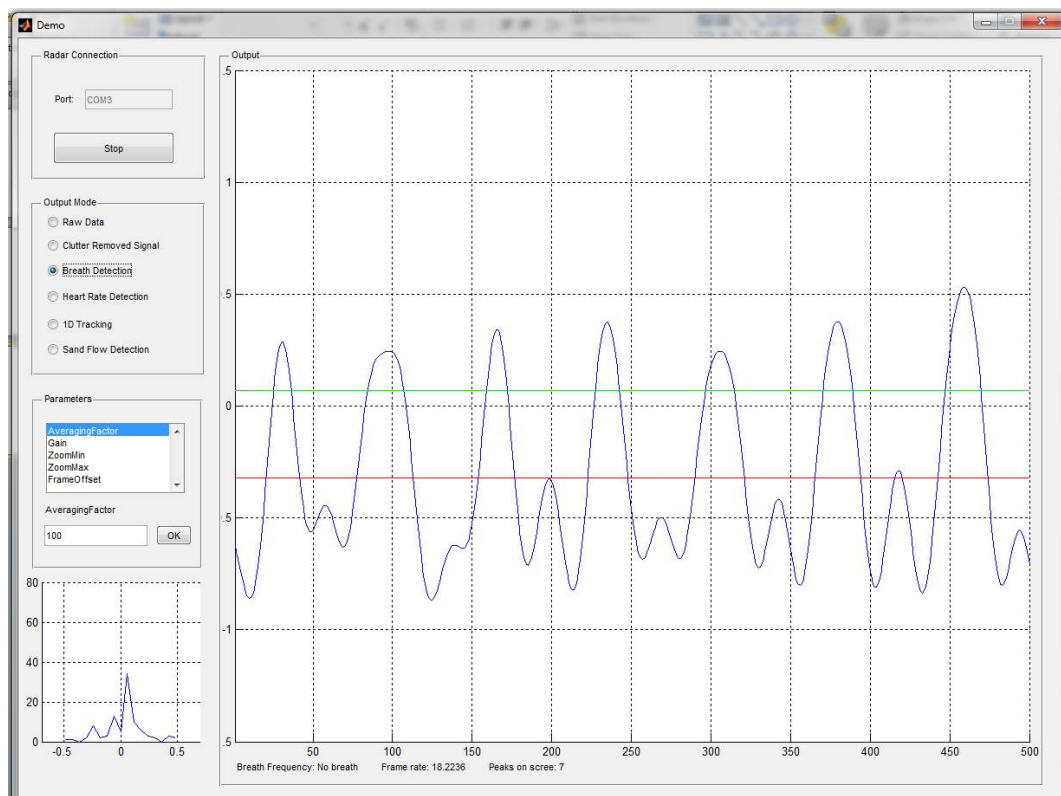


Figure 9-4 Screen shot during breath detection on a human in the radar range.

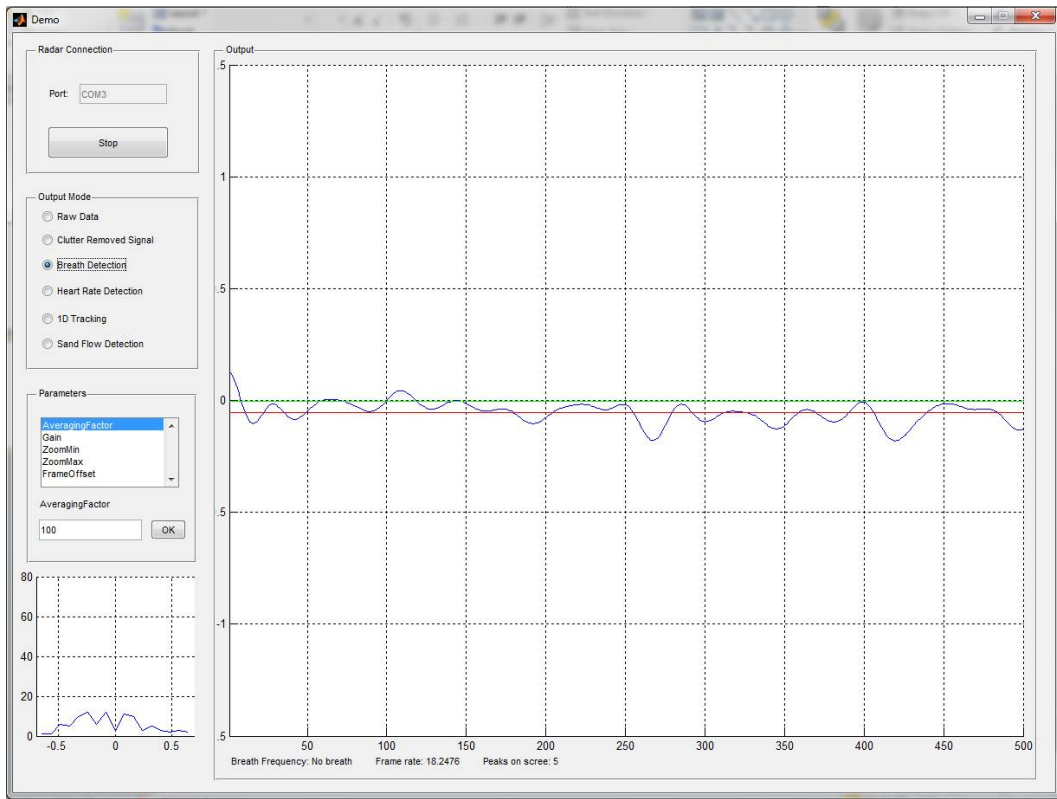


Figure 9-5 Screen shot during breath detection without any human in the radar range.

9.5 Heart Rate Detection

A function variant from the off line heart rate detection by wavelet packets. The function provides the heart rate in every n seconds (where n is adjustable) by a loop with following procedure:

- Collect signal for n seconds and save to a data matrix;
- Calculate the frame rate and other key value for further processing;
- Calculate the nodes that are needed for reconstruction;
- Detect heart rate;
- Drop the data matrix.

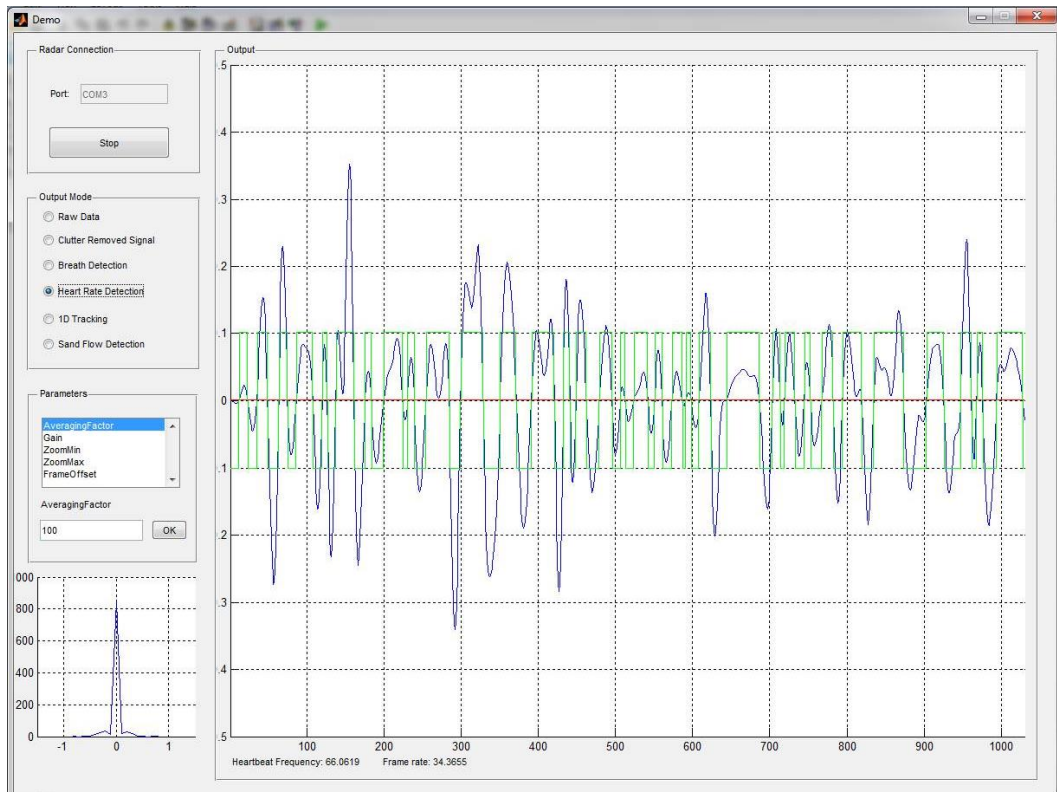


Figure 9-6 Screen shot during heart rate detection on a human in the radar range.

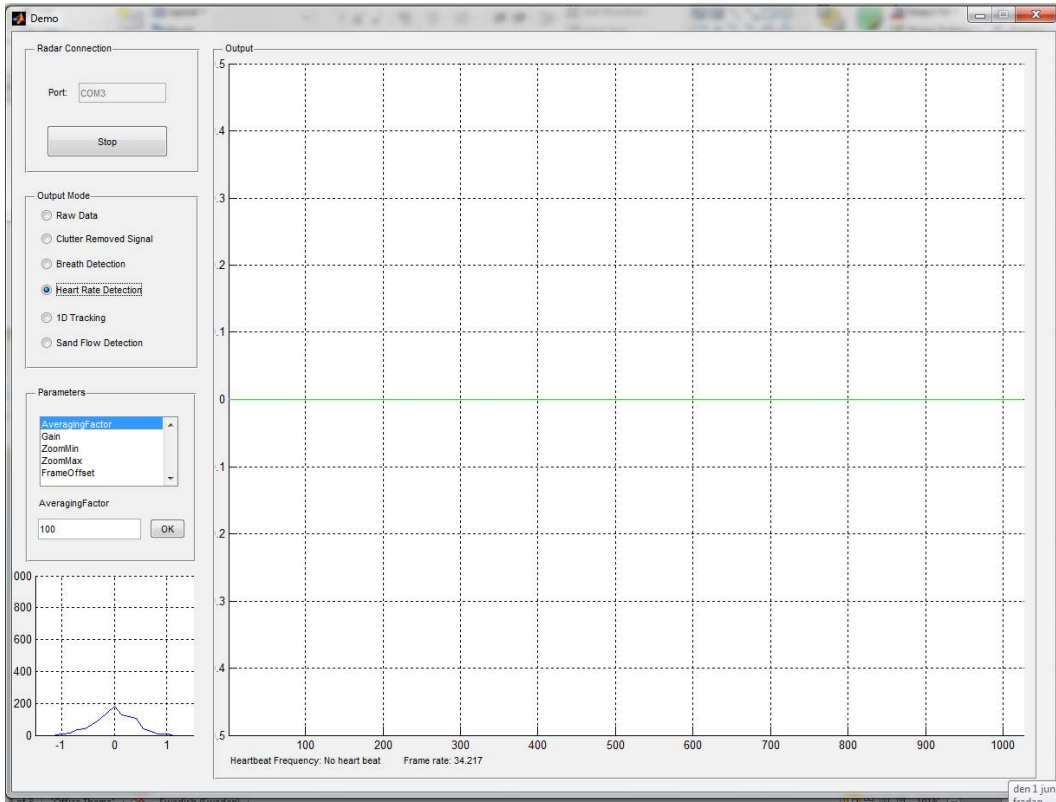


Figure 9-7 Screen shot during heart rate detection without any human in the radar range.

10 Appendix B: Paper Published in EuCAP 2014

There is a paper published in EuCAP 2014 regarding this work.

Detection of Breathing and Heartbeat by Using a Simple UWB Radar System

Qiuchi Jian*, Jian Yang*, Yinan Yu*, Peter Björkholm†, Tomas McKelvey*

*Dept. of Signals and systems, Chalmers University of Technology, SE-41296 Gothenburg, Sweden

qiuchi@student.chalmers.se, (jian.yang, yinan, mckelvey)@chalmers.se

†Acreo Swedish ICT AB, Gothenburg, Sweden, Peter.Bjorkholm@acreo.se

Abstract—We present the development on an ultra-wideband (UWB) radar system and its signal processing algorithms for detecting human breathing and heartbeat in the paper. The UWB radar system consists of two (Tx and Rx) antennas and one compact CMOS UWB transceiver. Several signal processing techniques are developed for the application. The system has been tested by real measurements.

Index Terms—UWB radar application; wavelet; empirical mode decomposition, breathing monitoring; heartbeat detection.

I. INTRODUCTION

Ultra-wideband (UWB) radars are widely used in different applications, such as through-wall tracking and detection [1], medical monitoring instruments [2], life detection [3], industry processing monitoring [4], etc. Several distinct advantages make UWB radar systems attractive: i) good time domain resolution and therefore accurate tracking and positioning; ii) strengthened target recognition; iii) robust immunity to passive jamming; iv) relatively low cost.

In this paper, a simple compact UWB radar system [5] is applied to the application of breathing and heartbeat detection. An experimental vibration system with a known frequency is set up as an emulating model for heartbeat in order to develop signal processing algorithms. Based on the experiment data and true human measurements, several signal processing algorithms, such as wavelet, empirical mode decomposition, are explored and implemented. Promising results are achieved.

II. SYSTEM CALIBRATION

System calibration is applied to clarify the system property and identify potential interferences that could compromise the measurements, such as temperature effect and jamming. The results conclude that the interferences could have significant impact on measurements of minor movement such as human heartbeat. Thus, adjustments corresponding to these have been done on the further experiment environment setups, including discarding data collected during heat up period and performing measurements in electromagnetic shielded environment.

III. BREATHING MONITORING

The setup for breathing detection is as shown in Fig. 1: two Vivaldi antennas are placed in parallel with $d_a = 12$ cm, and one person is sitting in a chair with a distance $d_{obj} = 24$ cm between the chest and the outer edge of the antennas.

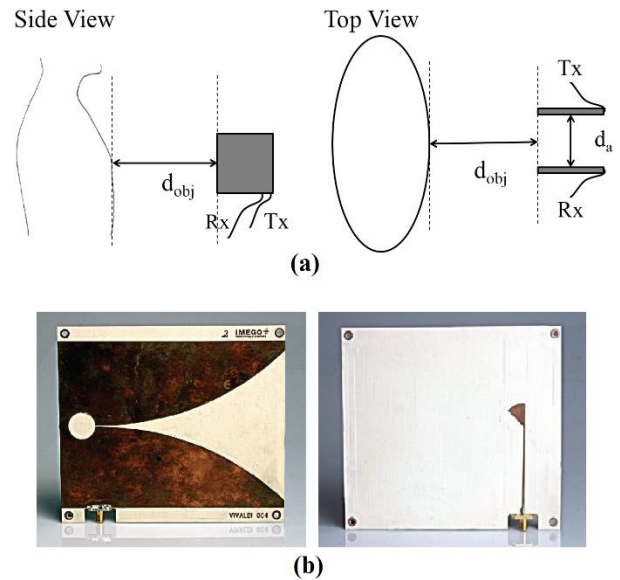


Figure 1. Experimental setup of breath detection (upper) and the Vivaldi antenna (lower).

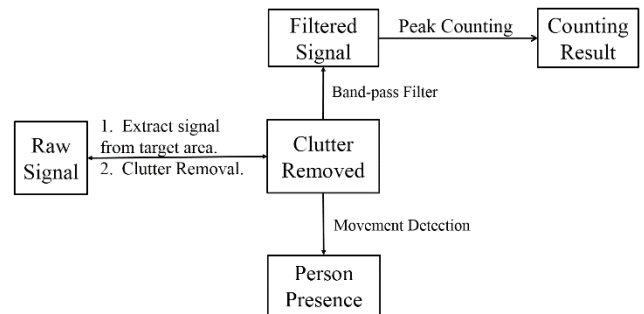


Figure 2. Signal processing procedure diagram for breath detection.

In the experiment phase, measurements have been done for 60 seconds continuously. Then the collected raw data has been processed following the procedure in Fig. 2.

As depicted in Fig.2, based on the distance between the human and the antennas, it is possible to extract signal from the area that covers the human's position. Then, by applying singular value decomposition method to remove the reflection from the static objects in the signal (please refer to [1]), an

enhanced clutter-removed signal is obtained. The clutter-removed signal is been further processed in order to do the movement detection as well as the breath signal reconstruction.

A differential phase method is applied here for movement detection: for two identical signals with a time delay, the time delay could be obtained by Fourier Transform [1].

Suppose s_1 and s_2 are identical signals with a phase shift:

$$s_2(\tau) = s_1(t - \tau) \quad (1)$$

By applying Fourier Transform we have:

$$S_1(\omega) = S_2(\omega) e^{-j\omega\tau} \quad (2)$$

Where τ is the time shift between two consecutive measurements, which is positive when the patient is exhaling and negative when inhaling. Therefore:

$$S_1(\omega) / S_2(\omega) = e^{-j\omega\tau} \quad (3)$$

Thus, the angel of $S_1(\omega) / S_2(\omega)$ could be obtained by:

$$\text{angel} = -j\omega\tau \quad (4)$$

Since human breath is a slow periodic movement, the statistical distribution of the reflection from the breathing chest is centered at a low frequency. Fig. 3 is the comparison of the movement detection results with and without presence of a person. The breathing can be detected by a simple Generalized Likelihood Ratio Test (GLRT).

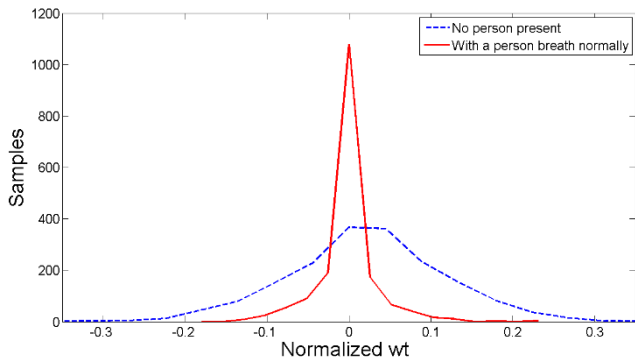


Figure 3. Signal extracted for movement detection.

Results from one minute continuous measurements can be found in Fig. 4. After preliminary processing, the breathing and heartbeat signals are assumed to be additive as shown in Fig. 4. The ‘envelop’ is considered as the breathing signal and the higher frequency components is the heartbeat.

IV. HEARTBEAT DETECTION

First, human heartbeat movements are emulated by using a vibrating corner reflector, as shown in Fig. 5. The experimental setup contains a function generator, a vibrator, a corner reflector, and our UWB system. To rule out jamming from other sources in order to develop and test signal processing (SP) algorithms in the early stage of the work, the experimental setup, except the desktop computer, was placed inside a magnetic shielded (MS) room. Different signal processing (SP)

techniques, including band-pass filtering, empirical mode decomposition (EMD) and wavelet packets, are explored and applied to different scenarios, as shown in Fig.6.

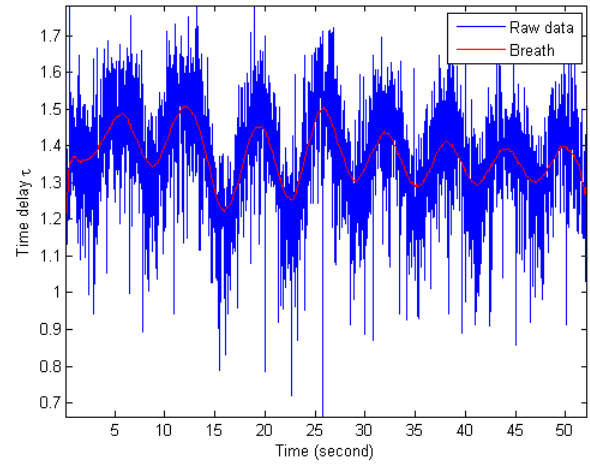


Figure 4. Breath signal reconstruction from measurements during 55 seconds.



Figure 5. Experimental setup of vibrating corner reflector.

The result of a moving metal plate with 1.5 Hz frequency is shown in Fig. 7. Although the reconstructed signals share high similarity in frequency domain, the signal processed by the FIR1 filter contains side lobes with higher amplitude. However, it can be used as a complementary approach in later experiments.

Then, the tested approaches are applied to the detection of human heartbeats with the same setup as breathing detection presented in Fig. 1 (a). The only difference is all measurements are done in MS room like the simulation experiment above in order to rule out Jamming. An adjusted signal processing flow was used, as shown in Fig.8.

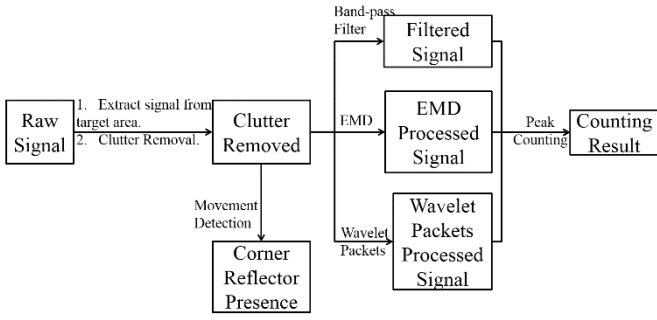


Figure 6. Signal processing procedure diagram for corner reflector movement detection.

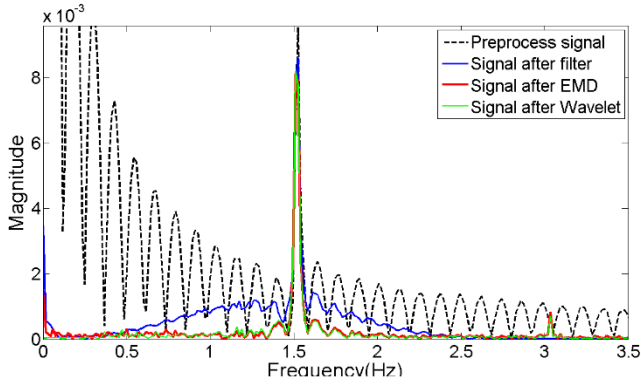


Figure 7. The results of signal of one sample with 1.5 Hz movement processed in the frequency domain.

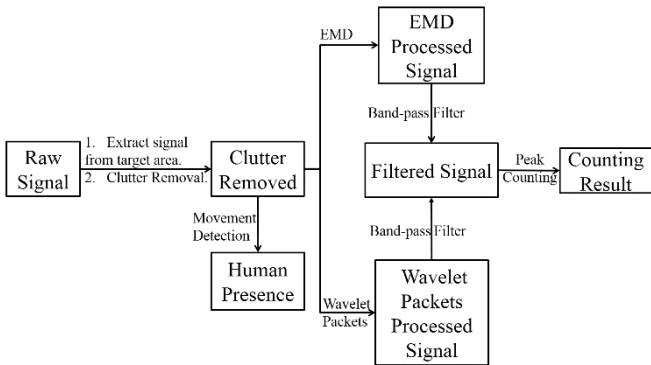


Figure 8. Signal processing procedure diagram for heartbeat detection.

As depicted in Fig. 8, two methods are applied to the clutter removed signal: EMD and Wavelet Packets. EMD is a nonlinear technique that can decompose a signal into finite components known as Instantaneous Mode Functions (IMF), which was developed by N.E. Huang in 1998. Specifically, the algorithm used in this paper achieves the target signal $s(t)$ decomposition by the following steps [6] :

- Find all minima and maxima extremes and plot a curve for each set by using cubic spline interpolation, which are the blue and red curves respectively.

- Compute the mean values between the maxima and minima curves, and make a residual curve $r(t)$ which is the pink one in the figure.
- Get the detail known as IMF by $d(t) = s(t) - m(t)$.
- Repeat the process above on the residual $r(t)$ until it fits the stopping criteria.

The stopping criteria can be defined based on the requirement of the analysis. In this project, an existing library is used for calculation which defines the calculation stops once all condition below are satisfied [7]:

- For each point, $\text{meanAmplitude}(t) < 0.5 * \text{amplitude}(t)$;
- $\text{mean of boolcriteria}(t)$ less than 0.05;
- There are less than two extremes in the curve.

where

$$\text{meanAmplitude}(t) = \frac{\text{abs}(\text{maxAmplitude}(t) + \text{minAmplitude}(t))}{2} \quad (5)$$

$$\text{amplitude}(t) = \frac{\text{abs}(\text{maxAmplitude}(t) - \text{minAmplitude}(t))}{2} \quad (6)$$

$$\text{boolcriteria}(t) = \frac{\text{meanAmplitude}(t)}{\text{amplitude}(t)} > 0.05 \quad (7)$$

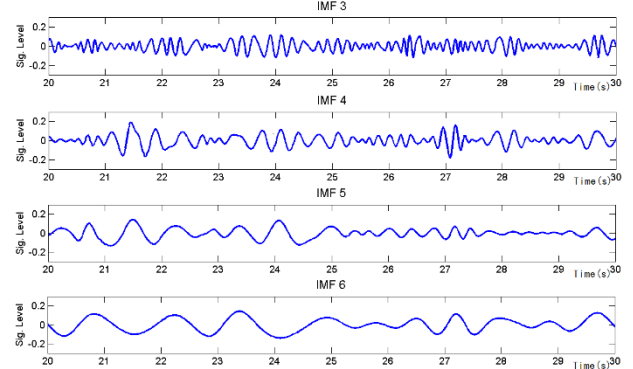


Figure 9. Four IMFs that decomposed from the clutter removed signal, which are used for heartbeat signal reconstruction.

Fig. 9 shows four IMFs that are decomposed from the clutter removed signal. By combining them together, a rough reconstructed heartbeat signal could be obtained [8].

Another technique is the wavelet decomposition. The wavelet decomposition is a technique for decomposing time series with different scales and times. [9] By using Wavelet transform, a signal could be divided into two parts: Signals in lower frequency (referred as A, which stands for 'Approximation coefficients') and higher frequency (referred as D, which stands for 'Details').

By using wavelet packets, the wavelet transform is first applied to the original signal to get A and D. Then the transform is applied again on both A and D and their outcome respectively. Hence, this analysis will produce a binary tree with root node on the top of the tree and $2n$ on the n th level of the tree. By doing this, the frequency components can be selected according to our interests.

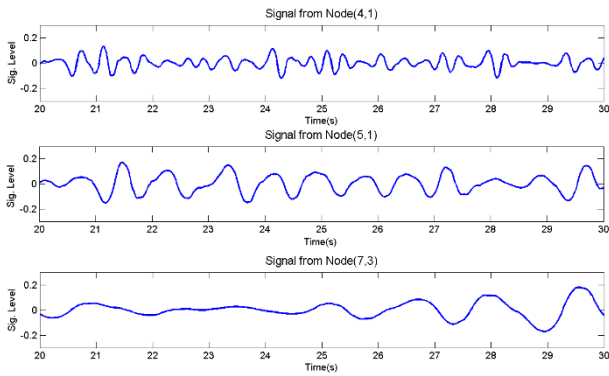


Figure 10. Three sub signal that decomposed from the clutter removed signal, which are used for heartbeat signal reconstruction. Node (4, 1) indicates the node is the 1st node on the 4th level of the binary tree.

Fig. 10 shows three nodes that are decomposed from the clutter removed signal. In order to reconstructed heartbeat signal, we can combine all signals from nodes that are within our interest frequency range.

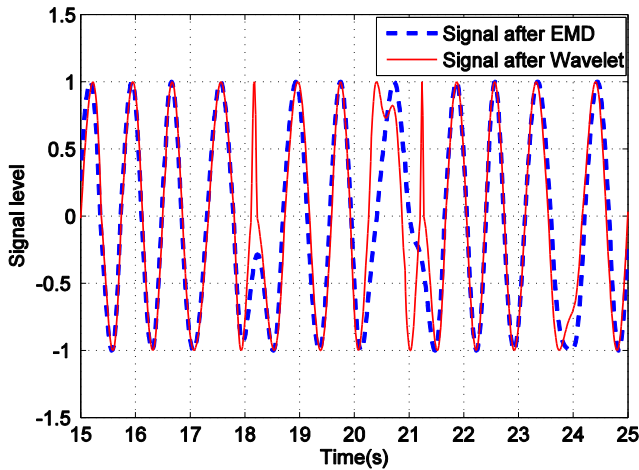


Figure 11. Heartbeat signal reconstruction from continuous measurements.

In the reality, the breathing and the heartbeat signals are additive together in the receiving signals, as shown in Fig. 4. The 'envelop' is considered as the breathing signal and the higher frequency components is the heartbeat which is of our interest. By applying EMD and wavelet packets methods, both the breathing and the unwanted components with higher frequencies than the heartbeat are sufficiently suppressed. One example of the reconstruction results in time domain is shown in Fig. 11. We can see that the outcome of both methods share high similarity on their shapes and synchronized at their peaks.

V. CONCLUSIONS

In this work, possible applications are implemented and tested using one UWB radar chip. Breath detection is one of the most promising possibilities for patient monitoring in an

open area or even through a wall due to its penetration ability. From the experiments using the corner reflector and measurements of real heartbeats, we conclude that it is possible to detect small movements with $\pm 0.5\text{mm}$ amplitude using the radar system. The wavelet packets and EMD methods are applied to suppress clutters and interference and the heartbeats are reconstructed by periodic sinusoid.

Although there are many previous studies focusing on certain vital signs [8] or signal to noise and clutter ratio improvement [10], but with the performance of current system, by combining different signal processing methods, the system can achieve effective measurement both off-line and in real time with less power and smaller antennas. Therefore, better mobility is achieved.

As future work, more radar modules can be utilized simultaneously to achieve better resolutions in two or three dimensions for ranging and tracking applications. By using the correlation between the signals from different radar modules, a higher signal to noise ratio could be obtained.

VI. REFERENCES

- [1] Yu, Yinan; Yang, Jian; McKelvey, Tomas; Stoew, Borys, "Compact UWB indoor and through-wall radar with precise ranging and tracking," *International Journal on Antenna and Propagations*, vol. 2012, Article ID 678590, 11 pages, 2012.
- [2] S. Abtahi, J. Yang, and S. Kidborg, "A new compact multiband antenna for stroke diagnosis system over 0.5–3 GHz," *Microwave and Optical Technology Lett.*, vol. 54, no. 10, pp. 2342–2346, October 2012.
- [3] B. Allen, M. Dohler, E. Okon, W. Malik, A. Brown, and D. Edwards, *Ultra wideband antennas and propagation for communications, radar and imaging*, Wiley.com, 2006.
- [4] S. S. Fayazi, H.-S. Lui, and J. Yang, "Microwave imaging of nearfieldobject using ultra-wideband synthetic aperture radar algorithm," in *Proc. 2012 IEEE Antennas and Propagation Society International Symposium*, 2012, pp. 1–2.
- [5] Y. Yu, S. Maalik, J. Yang, T. McKelvey, K. Malmstrom, L. Landen, and B. Stoew, "A new UWB radar system using UWB CMOS chip," in *Proc. 5th European Conference on Antennas and Propagation (EUCAP2011)*, 2011, pp. 771–775.
- [6] N. E. Huang, Z. Shen, S. R. Long, M. L. Wu, H. H. Shih, Q. Zheng, N. C. Yen, C. C. Tung and H. H. Liu: "The empirical mode decomposition and Hilbert spectrum for nonlinear and nonstationary time series analysis," *Proc. Roy. Soc. London A*, vol. 454, pp. 903–995, 1998.
- [7] Gabriel Rilling, Patrick Flandrin, Paulo Goncalves: *On Empirical Mode Decomposition and its Algorithms*, 1998.
- [8] E. P. Souza Neto, M. A. Custaud, C. J. Cejka, P. Abry, J. Frutoso, C. Gharib and P. Flandrin: "Assessment of cardiovascular autonomic control by the Empirical Mode Decomposition," in *Proc. 4th Int. Workshop on Biosignal Interpretation, Como (I)*, 2002, pp. 123-126.
- [9] Donald B., Percival & Andre T. Walden: *Wavelet Methods for Time Series Analysis*, 2000.
- [10] A. Nezirovic, A. G. Yarovoy, and L. P. Ligthart, "Signal processing for improved detection of trapped victims using UWB radar," *IEEE Transactions on Geoscience and Remote Sensing*, vol. 48, no. 4, pp. 2005-2014.

